Inorganic Chemistry

Article

pubs.acs.org/IC

Binary Group 15 Polyazides. Structural Characterization of $[Bi(N_3)_4]^-$, $[Bi(N_3)_5]^{2-}$, $[bipy{\cdot}Bi(N_3)_5]^{2-}$, $[Bi(N_3)_6]^{3-}$, $bipy{\cdot}As(N_3)_3$, $bipy{\cdot}Sb(N_3)_3$, and $[(bipy)_2{\cdot}Bi(N_3)_3]_2$ and on the Lone Pair Activation of Valence Electrons†

Ralf Haiges,*[,‡] Martin Rahm,*[,‡] David A. Dixon,[§] Edward B. Garner, III,[§] and Karl O. Christe*[,‡]

[‡]Loker Hydrocarbon Research Institute and Department of Chemistry, University of Southern California, Los Angeles, California 90089, United States

[§]Department of Chemistry, University of Alabama, Tuscaloosa, Alabama 35487-0336, United States

Supporting Information

ABSTRACT: The binary group 15 polyazides $As(N_3)_3$, $Sb(N_3)_3$, and $Bi(N_3)_3$ were stabilized by either anion or donor−acceptor adduct formation. Crystal structures are reported for $[Bi(N_3)_4]^-$, $[Bi(N_3)_5]^{2-}$, $[bipy{\cdot}Bi(N_3)_5]^{2-}$, $[Bi(N_3)_6]^{3-}$, $bipy{\cdot}As(N_3)_3$, $bipy{\cdot}Sb(N_3)_3$, and $[(bipy)_2{\cdot}Bi(N_3)_3]_2$. The lone valence electron pair on the central atom of these pnictogen(+III) compounds can be either sterically active or inactive. The $[Bi(N_3)_5]^{2-}$ anion possesses a sterically active lone pair and a monomeric pseudo-octahedral structure with a coordination number of 6, whereas its 2,2′-bipyridine adduct exhibits a pseudo-monocapped trigonal prismatic structure with CN 7 and a sterically inactive lone pair. Because of the high oxidizing power of Bi(+V), reactions aimed at $Bi(N_3)_5$ and $[Bi(N_3)_6]^-$ resulted in the reduction to bismuth(+III) compounds by $[N_3]^-$. The powder X-ray diffraction pattern of $Bi(N_3)_3$ was recorded at 298 K and is distinct from that calculated for $Sb(N_3)_3$ from its single-crystal data at 223 K. The $[(bipy)_2{\cdot}Bi(N_3)_3]_2$ adduct is dimeric and derived from two BiN_8 square antiprisms sharing an edge consisting of two $\mu^{1,1}$-bridging N_3 ligands and with bismuth having CN 8 and a sterically inactive lone pair. The novel $bipy{\cdot}As(N_3)_3$ and $bipy{\cdot}Sb(N_3)_3$ adducts are monomeric and isostructural and contain a sterically active lone pair on their central atom and a CN of 6. A systematic quantum chemical analysis of the structures of these polyazides suggests that the M06-2X density functional is well suited for the prediction of the steric activity of lone pairs in main-group chemistry. Furthermore, it was found that the solid-state structures can strongly differ from those of the free gas-phase species or those in solutions and that lone pairs that are sterically inactive in a chemical surrounding can become activated in the free isolated species.

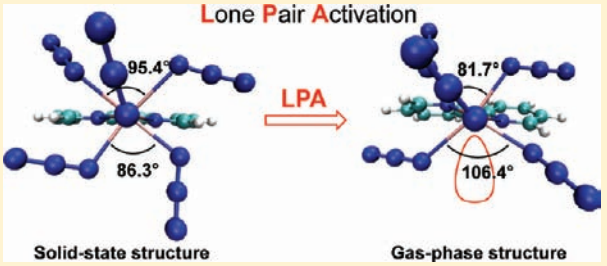

INTRODUCTION

Inorganic polyazido compounds and their chemistry have received a great deal of attention in recent years.[1−25] The heats of formation of polyazides are highly positive, and their energy content generally increases with an increase in the number of azido ligands. Therefore, it is not surprising that polyazido compounds have great potential as energetic materials. For example, lead diazide is widely used as the primary explosive in propellants and explosives. However, the use of this compound releases toxic lead into the environment. Because of the environmental hazards and human toxicity issues associated with the production and use of lead diazide, there is great interest in new, environmentally benign, and nontoxic energetic materials that could serve as a drop-in replacement for lead diazide. The low toxicity and environmentally benign character of bismuth renders it an ideal replacement for lead in this application. As a consequence, we have for the past several years systematically studied the synthesis and characterization of binary bismuth and related group 15 polyazides.

With the syntheses of $P(N_3)_3$,[12a] $P(N_3)_5$,[12a] $[P(N_3)_6]^-$,[12b,c] $As(N_3)_3$,[9,12d,e] $[As(N_3)_4]^-$,[6] $As(N_3)_5$,[11] $[As(N_3)_4]^+$,[6] $[As(N_3)_6]^-$,[6,12f] $Sb(N_3)_3$,[9,12g] $[Sb(N_3)_4]^-$,[6] $Sb(N_3)_5$,[11] $[Sb(N_3)_4]^+$,[6] and $[Sb(N_3)_6]^-$,[6,11] a significant number of binary polyazido compounds of the lighter elements of group 15 have been prepared, although only $[P(N_3)_6]^-$,[12c] $As(N_3)_3$,[9] $[As(N_3)_6]^-$,[6,12f] $Sb(N_3)_3$,[9] and $[Sb(N_3)_6]^-$[11] have been structurally characterized. However, the situation has been quite different for bismuth, for which, until one year ago, only the formation of an inseparable mixture of $Bi(N_3)_3$ and AgI had been reported.[21] Very recently, the syntheses of $Bi(N_3)_3$,[23,24] $[P(C_6H_5)_4]^+[Bi(N_3)_4]^-$,[23] $[P(C_6H_5)_4)^+]_3[Bi(N_3)_6]^{3-}$,[23] and $Bi(N_3)_3{\cdot}2py$[24] (py = pyridine) have been described, and structural characterizations were given for $[P(C_6H_5)_4)^+]_3[Bi(N_3)_6]^{3-}$,[23] $[P(C_6H_5)_4]^+[Bi(N_3)_4]^-$,[23] and $Bi(N_3)_3{\cdot}2py$.[24] These publications prompt us to communicate in this paper our own results, which had been reported previously at some conferences but

Received: October 24, 2011
Published: December 23, 2011

   dx.doi.org/10.1021/ic202307a | *Inorg. Chem.* 2012, 51, 1127−1141

have not been summarized so far for publication. We also describe general structural relationships in group 15 azides and the results from electronic structure calculations.

EXPERIMENTAL SECTION

Caution! *Many of the polyazides of this work, and particularly* $Bi(N_3)_3$*, are extremely shock-sensitive and can explode violently upon the slightest provocation. They should be handled only on a scale of less than 1 mmol using appropriate safety precautions.*[16] ***Ignoring safety precautions can lead to serious injuries!***

Materials and Apparatus. All reactions were carried out in Teflon-FEP ampules that were closed by stainless steel valves. Volatile materials were handled in a Pyrex glass vacuum line. Nonvolatile materials were handled in the dry nitrogen atmosphere of a glovebox. Raman spectra were recorded in the Teflon-FEP reactors in the range 4000−80 cm^{-1} on a Bruker Equinox 55 FT-RA spectrophotometer using a Nd:YAG laser at 1064 nm with ***power levels of less than 50 mW***. IR spectra were recorded in the range 4000−400 cm^{-1} on a Midac, M Series, FT-IR spectrometer using KBr pellets. The pellets were prepared inside the glovebox using an Econo mini-press (Barnes Engineering Co.). SbF_3, BiF_3 (both Ozark Mahoning), and 2,2′-bipyridine (Aldrich) were used without further purification. AsF_3 (Advanced Research Chemicals) and Me_3SiN_3 (Aldrich) were purified by fractional condensation prior to use. Solvents were dried by standard methods and freshly distilled prior to use. $P(C_6H_5)_4N_3$ and $PNPN_3$ were prepared by ion exchange from $P(C_6H_5)_4Cl$ and PNPCl, respectively.[25]

Preparation of $Bi(N_3)_3$. Method 1: A sample of BiF_3 (0.41 mmol) was loaded into a Teflon-FEP ampule, followed by the addition of acetonitrile (60 mmol) and Me_3SiN_3 (4.0 mmol) in vacuo at −196 °C. The mixture was allowed to warm to ambient temperature. After 16 h at ambient temperature and occasional agitation, a colorless liquid over an off-white precipitate was obtained. The temperature was lowered to −20 °C, and all volatile material was pumped off. After additional pumping for 24 h at ambient temperature, a pale-yellow solid was obtained (145 mg; weight expected for 0.41 mmol of $Bi(N_3)_3$, 137 mg). **Method 2:** A sample of BiF_5 (0.2 mmol) was loaded into a Teflon-FEP ampule, followed by the addition of acetonitrile (60 mmol) and Me_3SiN_3 (3.0 mmol) in vacuo at −196 °C. The mixture was allowed to warm to ambient temperature. During the warmup, the solution bubbled and evolved gas. After 30 min at ambient temperature, a colorless liquid above an off-white precipitate was obtained. The temperature was lowered to −20 °C, and all volatile material was pumped off. After additional pumping for 24 h at ambient temperature, a pale-yellow solid was obtained (73 mg; weight expected for 0.2 mmol of $Bi(N_3)_3$, 67 mg).

Raman (15 mW, −80 °C): $\tilde{\nu}$ 2128 (0.9), 2115 (7.0), 2085 (0.9), 2064 (1.5), 2043 (10.0), 2016 (0.4), 1367 (0.2), 1335 (3.7), 1282 (0.8), 1272 (0.3), 656 (0.8), 608 (0.5), 398 (1.2), 342 (3.4), 297 (0.8), 276 (1.0), 232 (2.3), 212 (2.5), 195 (0.3), 183 (0.8), 160 (1.4), 137 (2.9), 120 (2.7), 100 (0.8), 87 (2.3) cm^{-1}; bands belonging to a residual amount of CH_3CN, $\tilde{\nu}$ 2998 (1.5), 2935 (8.3), 2722 (0.3), 2296 (0.3), 2254 (3.9), 1355 (0.3), 925 (0.6), 388 (0.4). IR (KBr, 20 °C): $\tilde{\nu}$ 2055 vs, 2037 sh, 1321 m, 1270 mw, 644 w, 593 vw, 530 w, 463 w, 421 w cm^{-1}.

Preparation of $[(bipy)_2{\cdot}Bi(N_3)_3]_2$. In a Teflon-FEP ampule, CH_3CN (100 mmol) and Me_3SiN_3 (3.0 mmol) were condensed at −196 °C in vacuo on top of a mixture of BiF_5 (0.4 mmol) and 2,2′-bipyridine (0.8 mmol). The mixture was allowed to warm to ambient temperature. During the warmup, the solution bubbled with gas evolution. After 30 min at ambient temperature and some agitation, a pale-yellow solution was obtained. The temperature was lowered to −20 °C, and all volatile material was pumped off. A yellow crystalline solid was obtained (264 mg; weight expected for 0.2 mmol of $[(bipy)_2{\cdot}Bi(N_3)_3]_2$, 259 mg).

Raman (15 mW, −50 °C): $\tilde{\nu}$ 3086 (4.6), 3076 (5.1), 3065 (3.5), 3049 (1.3), 2079 (0.6), 2049 (4.3), 2039 (0.1), 2025 (3.1), 2012 (0.7), 1660 (0.1), 1602 (3.4), 1592 (10.0), 1572 (4.0), 1493 (4.3), 1449 (1.0), 1432 (0.8), 1325 (6.0), 1312 (7.2), 1286 (1.4), 1277 (0.4), 1264 (0.4), 1248 (0.2), 1239 (0.3), 1178 (0.1), 1159 (0.5), 1154 (0.5), 1080 (0.3), 1065 (2.8), 1044 (0.6), 1011 (5.4), 998 (2.0), 896 (0.1), 819 (0.2), 809 (0.2), 767 (2.5), 741 (0.2), 645 (1.5), 625 (0.5), 550 (0.1), 449 (0.1), 430 (0.1), 413 (0.1), 352 (2.4), 304 (4.1), 262 (0.8), 253 (1.0), 248 (1.0), 235 (0.8), 211 (0.8), 192 (0.5), 175 (0.5), 137 (2.8), 121 (1.6), 109 (3.0) cm^{-1}.

Preparation of bipy·$M(N_3)_3$ (M = As, Sb). In a Teflon-FEP ampule, Me_3SiN_3 (8.0 mmol) was condensed at −196 °C in vacuo on top of a frozen solution of MF_3 (2.0 mmol) and 2,2′-bipyridine (2.0 mmol). The mixture was allowed to warm to ambient temperature. After 30 min at ambient temperature, a clear colorless solution was obtained. The temperature was lowered to −20 °C, and all volatile material was pumped off, leaving behind colorless crystalline solids. Weights expected for 2.00 mmol of bipy·$As(N_3)_3$ and bipy·$Sb(N_3)_3$: 0.714 and 0.808 g. Weights found: 0.718 and 0.799 g, respectively.

bipy·$As(N_3)_3$. Raman (35 mW, 20 °C): $\tilde{\nu}$ 3076 (5.9), 2118 (4.2), 2091 (1.2), 2076 (1.4), 2057 (0.7), 1647 (0.2), 1616 (0.5), 1591 (4.0), 1576 (2.1), 1488 (2.8), 1450 (0.8), 1440 (0.3), 1309 (4.0), 1280 (1.5), 1258 (0.7), 1239 (0.6), 1220 (0.1), 1176 (0.3), 1158 (0.6), 1104 (0.1), 1097 (0.2), 1062 (1.8), 1048 (0.9), 1003 (4.2), 892 (0.1), 814 (0.2), 767 (2.0), 678 (0.7), 667 (0.7), 653 (0.4), 636 (0.1), 621 (0.5), 558 (0.1), 472 (sh), 462 (5.8), 413 (1.2), 405 (2.4), 377 (2.0), 341 (0.3), 336 (0.2), 290 (0.7), 250 (1.3), 214 (1.1), 192 (0.1), 107 (10.0) cm^{-1}.

bipy·$Sb(N_3)_3$. Raman (100 mW, 20 °C): $\tilde{\nu}$ 3076 (7.5), 2108 (1.7), 2097 (2.2), 2081 (0.1 sh), 2071 (1.8), 2065 (0.3 sh), 2050 (0.4), 2035 (0.4), 1613 (2.2), 1598 (10.0), 1593 (9.8), 1575 (5.7), 1569 (5.7), 1502 (2.2), 1492 (2.9), 1486 (2.1), 1449 (2.4), 1435 (0.7), 1324 (8.3), 1311 (6.2), 1285 (1.8), 1279 (1.5), 1262 (0.5), 1238 (1.8), 1217 (0.1), 1173 (0.5), 1162 (1.4), 1152 (0.7), 1095 (0.3), 1079 (0.2), 1065 (2.6), 1046 (2.4), 1027 (3.0), 1006 (3.4), 997 (5.6), 897 (0.2), 809 (0.5), 769 (3.4), 745 (0.1), 662 (0.8), 656 (0.9), 653 (0.9), 643 (0.5), 638 (0.5), 618 (1.0), 588 (0.7), 556 (0.5), 547 (0.2 sh), 500 (4.0), 456 (3.6), 432 (0.3), 419 (4.3), 401 (3.6), 364 (3.3), 348 (0.5), 332 (0.5), 320 (0.4), 279 (0.8), 237 (3.1), 215 (0.5), 200 (0.5), 179 (1.0) cm^{-1}.

Preparation of $A[Bi(N_3)_4]$, $A_2[Bi(N_3)_5]$ (A = $P(C_6H_5)_4$, PNP), and $[P(C_6H_5)_4]_3[Bi(N_3)_6]$ Salts. Under a stream of dry nitrogen, a stoichiometric amount of AN_3 was added to a frozen mixture of $Bi(N_3)_3$ (0.30 mmol) in CH_3CN (40 mmol) at −64 °C. The reaction mixture was kept at −25 °C for 30 min, occasionally agitated, and then warmed to ambient temperature. After about 60 min, the initial precipitate of $Bi(N_3)_3$ had dissolved and a yellow solution was obtained. The solution was cooled to −20 °C, and all volatiles were removed in a dynamic vacuum, leaving behind pale-yellow crystalline solids. Weights expected for 0.30 mmol of $[P(C_6H_5)_4][Bi(N_3)_4]$, $[PNP][Bi(N_3)_4]$, $[P(C_6H_5)_4]_2[Bi(N_3)_5]$, $[PNP]_2[Bi(N_3)_5]$, and $[P(C_6H_5)_4]_3[Bi(N_3)_6]$: 0.215, 0.275, 0.329, 0.449, and 0.444 g. Weights found: 0.226, 0.283, 0.321, 0.453, and 0.435 g, respectively.

$[P(C_6H_5)_4][Bi(N_3)_4]$. Raman (70 mW, 20 °C): $[Bi(N_3)_4]^-$, $\tilde{\nu}$ 2089 (4.8), 2038 (6.0), 2022 (0.5), 1328 (3.0), 1319 (0.8), 1280 (0.4), 1270 (0.5), 652 (0.9), 644 (0.9), 342 (10.0), 324 (4.2), 292 (3.5), 192 (0.5), 168 (1.5) cm^{-1}; $[P(C_6H_5)_4]^+$, $\tilde{\nu}$ 3173 (0.2), 3147 (0.2), 3070 (7.0), 3063 (6.9), 3010 (0.2), 2962 (0.3), 1590 (4.5), 1577 (1.0), 1487 (0.1), 1442 (0.3), 1193 (0.7), 1166 (0.4), 1110 (0.8), 1101 (2.0), 1031 (2.5), 1004 (8.8), 934 (0.2), 731 (0.4), 682 (1.6), 618 (1.1), 255 (1.0) cm^{-1}. IR (KBr, 25 °C): $[Bi(N_3)_4]^-$, $\tilde{\nu}$ 2059 sh, 2038 vs, 2023 sh, 1315 ms, 1265 m, 650 sh, 638 w, 617 vw, 603 w cm^{-1}; $[P(C_6H_5)_4]^+$, $\tilde{\nu}$3082 vw, 3057 vw, 1585 w, 1481 mw, 1437 m, 1190 w, 1160 w, 1107 ms, 1025 vw, 996 mw, 851 vw, 753 w, 723 ms, 689 ms, 528 s cm^{-1}.

$[PNP]_2[Bi(N_3)_5]$. Raman (60 mW, 20 °C): $[Bi(N_3)_6]^{3-}$, $\tilde{\nu}$ 2082 (1.5), 2041 (0.2), 2029 (0.3), 2020 (0.6), 1330 (1.1), 1318 (0.9), 1266 (0.1), 656 (0.2), 638 (0.5), 379 (3.8), 298 (1.3), 198 (0.4) cm^{-1}; $[PNP]^+$, $\tilde{\nu}$ 3176 (0.4), 3145 (0.5), 3060 (10.0), 3016 (0.3), 2997 (0.2), 2962 (0.4), 1590 (3.2), 1577 (1.1), 1483 (0.1), 1442 (0.3), 1184 (0.8), 1164 (0.9), 1113 (2.0), 1077 (0.1), 1029 (2.9), 1003 (6.9), 731 (0.2), 666 (2.0), 618 (1.3), 550 (0.1), 489 (0.1), 284 (0.4), 268 (0.3), 251 (0.6), 237 (1.1) cm^{-1}. IR (KBr, 20 °C): $[Bi(N_3)_5]^{2-}$, $\tilde{\nu}$ 2077 s, 2038 sh, 2016 vs, 1998 sh, 1313 m, 1299 m, 1286 m, 637 vw cm^{-1}; $[PNP]^+$, $\tilde{\nu}$ 3056 vw, 1587 w, 1573 vw, 1482 w; 1437 ms, 1286 m, 1266 m, 1182 w, 1161 vw, 1115 s, 1025 vw, 997 mw, 862 vw, 796 w, 758 mw, 747 m, 692 m, 723 s, 692 ms, 616 vw, 548 s, 535 ms, 499 m, 455 vw, cm^{-1}.

dx.doi.org/10.1021/ic202307a | Inorg. Chem. 2012, 51, 1127−1141

$[P(C_6H_5)_4]_3[Bi(N_3)_6]$. Raman (70 mW, 20 °C): $[Bi(N_3)_6]^{3-}$, $\tilde{\nu}$ 2065 (2.1), 2026 (0.7), 2010 (0.4), 1325 (2.8), 638 (0.5), 619 (1.5), 325 (4.8), 295 (1.4) cm^{-1}; $[P(C_6H_5)_4]^+$, $\tilde{\nu}$ 3176 (0.4), 3145 (0.6), 3064 (10.0), 2993 (0.5), 2965 (0.5), 1588 (3.8), 1578 (1.5), 1484 (0.1), 1443 (0.3), 1191 (0.8), 1167 (0.7), 1101 (2.0), 1032 (3.8), 1003 (8.9), 727 (0.5), 683 (1.5), 619 (1.5), 259 (2.5), 200 (1.2) cm^{-1}. IR (KBr, 20 °C): $[Bi(N_3)_6]^{3-}$, $\tilde{\nu}$ 2061 m, 2035 sh, 2003 vs, 1263 w, 637 vw cm^{-1}; $[P(C_6H_5)_4]^+$, $\tilde{\nu}$ 3084 vw, 3056 w, 1583 w, 1481 mw; 1436 m, 1261 vw, 1187 w, 1163 w, 1107 s, 1027 vw, 996 mw, 874 w, 760 mw, 753 s, 691 ms, 614 vw, 528 s cm^{-1}.

Preparation of $[P(C_6H_5)_4^+]_2[bipy{\cdot}Bi(N_3)_5]^{2-}$. BiF_3 (0.30 mmol), $P(C_6H_5)_4N_3$ (0.60 mmol), and 2,2′-bipyridine (0.30 mmol) were loaded into a Teflon-FEP ampule, followed by the addition of acetonitrile (100 mmol) and Me_3SiN_3 (4.0 mmol) in vacuo at −196 °C. The mixture was allowed to warm to ambient temperature. After 16 h at ambient temperature and occasional agitation, a pale-yellow solution was obtained. The temperature was lowered to −20 °C, and all volatile material was pumped off, resulting in the isolation of yellow crystals (385 mg; weight expected for 0.30 mmol of $[P(C_6H_5)_4][Bi(N_3)_5]$, 376 mg).

Raman (50 mW, −40 °C): $\tilde{\nu}$ 3061 (10.0), 2115 (0.3), 2088 (0.4), 2063 (2.5), 2044 (0.9), 2028 (0.6), 2011 (0.1), 1590 (6.2), 1577 (1.8), 1572 (1.7), 1489 (0.8), 1437 (0.3), 1429 (0.4), 1335 (2.7), 1325 (2.6), 1311 (2.3), 1281 (0.8), 1258 (0.2), 1246 (0.2), 1191 (0.6), 1167 (0.5), 1156 (0.4), 1113 (0.9), 1101 (1.7), 1080 (0.2), 1064 (1.0), 1030 (2.8), 1003 (8.1), 815 (0.2), 767 (1.0), 727 (0.8), 681 (1.1), 650 (0.5), 640 (0.6), 618 (1.0), 442 (0.1), 347 (1.6), 320 (4.2), 297 (0.1, sh), 282 (0.1, sh), 264 (2.1), 236 (0.3), 208 (1.4), 200 (0.5, sh), 179 (0.5, sh) cm^{-1}.

Crystal Structure Determinations. The single-crystal X-ray diffraction data for $[P(C_6H_5)_4][Bi(N_3)_4]$, $[PNP]_2[Bi(N_3)_5]$, $[P(C_6H_5)_4]_3[Bi(N_3)_6]$, $[P(C_6H_5)_4]_2[bipy{\cdot}Bi(N_3)_5]$, and $[(bipy)_2{\cdot}Bi(N_3)_3]_2$ were collected on a Bruker SMART APEX three-circle platform diffractometer, equipped with an APEX CCD detector with the χ axis fixed at 54.74°, and using Mo Kα radiation (graphite monochromator) from a fine-focus tube. The diffractometer was equipped with an LT-3 apparatus for low-temperature data collection using controlled liquid-nitrogen boil-off. A complete hemisphere of data was scanned on ω (0.3°) with a run time of 10 s per frame at a detector resolution of 512 × 512 pixels using the *SMART* software package.[26] A total of 1271 frames were collected in three sets, and a final set of 50 frames, identical with the first 50 frames, was also collected to determine any crystal decay. The frames were then processed using the *SAINT* software package[26] to give the *hkl* files corrected for Lp/decay (Lp = Lorentz and polarization correction). The absorption correction was performed using the *SADABS* program.[26] The structures were solved by the Patterson method using the *SHELX-90* program and refined by the least-squares method on F^2.[26] All non-hydrogen atoms were refined anisotropically.

The single-crystal X-ray diffraction data of $bipy{\cdot}As(N_3)_3$ and $bipy{\cdot}Sb(N_3)_3$ were collected on a Bruker SMART APEX DUO three-circle platform diffractometer, equipped with an APEX II CCD detector with the χ axis fixed at 54.74°, and using Mo Kα radiation (TRIUMPH curved-crystal monochromator) from a fine-focus tube. The diffractometer was equipped with an Oxford Cryosystems Cryostream 700 apparatus for low-temperature data collection. A complete hemisphere of data was scanned on ω (0.5°) with a run time of 1 s per frame at a detector resolution of 512 × 512 pixels using the *BIS* software package.[27] A total of 1464 frames were collected in four sets. The frames were then integrated using the *SAINT* algorithm[27] to give the *hkl* files corrected for Lp/decay. The absorption correction was performed using the *SADABS* program.[27] The structures were solved by the direct method and refined on F^2 using the Bruker *SHELXTL* software package.[27] All non-hydrogen atoms were refined anisotropically.

ORTEP drawings were prepared using the *ORTEP-3 for Windows V2.02* program.[28]

Computational Methods. Structure optimization and frequency analyses were performed using the recent hybrid meta exchange-correlation density functional (DFT) M06-2X[29] in *Gaussian 09*.[30] M06-2X has been shown to be reliable for calculating main-group thermochemistry.[29,31,32] Unpublished work by our group has also shown M06-2X to be superior to older DFT hybrid methods, such as B3LYP, in capturing the geometric effects of sterically active lone valence electron pairs in main-group compounds. One example of M06-2X's superiority to B3LYP is found for the IF_6^- and BrF_6^- anions. In this case, the experimentally found C_{3v} structure of IF_6^- and O_h structure of BrF_6^- are correctly predicted by M06-2X, whereas B3LYP predicts O_h symmetry for both. The obtained geometries are in excellent agreement with experimental values and even appear to (perhaps fortuitously) exceed the quality of coupled cluster CCSD(T)/aug-cc-pVTZ calculations[33] (see the Supporting Information). In some cases, the effect of solvation on the free isolated molecules was modeled using the using the self-consistent reaction field approach, as implemented in the polarizable continuum model (PCM) approximation in *Gaussian 09* with acetonitrile as the solvent.[34]

The bismuth atoms were described by the recent pseudo-potential-based core−valence correlation-consistent cc-pwCVTZ-PP basis set.[35] This basis set includes a Stuttgart energy-consistent, small-core, relativistic pseudo-potential, which replaces 60 core electrons of bismuth. The outer electrons are described by a (19s22p11d3f1g)/[7s6p5d3f1g] contracted basis set. All lighter elements were treated by Dunning's slightly smaller cc-pVTZ basis set.[36]

For the much larger $[(bipy)_2{\cdot}Bi(N_3)_3]_2$ complex, the bismuth center was instead described using the cc-pwCVDZ-PP basis set, which corresponds to a (15s12p7d1f)/[5s4p3d1f] Gaussian contraction of the outer electrons. For this species, all lighter elements were treated using Dunning's cc-pVDZ basis set.[36] The same basis set was used for all PCM optimizations. Second-derivative calculations were performed at all levels of theory to confirm that the optimized structures were local minima on the potential energy surfaces (PESs) and to provide vibrational frequencies.

To ensure that no artifacts arose because of the use of differently sized basis sets (on bismuth vs the ligand atoms), the structure of $[bipy{\cdot}Bi(N_3)_5]^{2-}$ was also optimized using the cc-pwCVDZ basis set on the ligand atoms, with the corresponding basis set on bismuth. This did not result in any geometrical changes compared to cc-pwCVDZ on bismuth and cc-pVDZ on nitrogen, carbon, and hydrogen. Furthermore, all species showed only very small geometry changes when the basis set was increased from the double-ζ to the triple-ζ level.

A natural bond order (NBO) analysis of the $[Bi(N_3)_6]^{3-}$ anion was performed on its M06-2X/cc-pwCVTZ-PP wave function, using *NBO*, version 3, in *Gaussian 09*.

RESULTS AND DISCUSSION

Syntheses of Bismuth, Arsenic, and Antimony Polyazides. By analogy with our previous syntheses of arsenic and antimony azides,[9,11] bismuth fluorides were reacted with an excess of Me_3SiN_3 in an acetonitrile solution. This resulted in rapid and complete fluoride−azide exchange and easy product separation. In the case of BiF_3, a pale-yellow precipitate of $Bi(N_3)_3$ (eq 1) was obtained.

$$BiF_3 + 3Me_3SiN_3 \xrightarrow{CH_3CN} Bi(N_3)_3 + 3Me_3SiF \qquad (1)$$

Similar reaction conditions had also been used by Villinger and Schulz[23] and Schulz and co-workers,[24] and their reported physical and spectroscopic properties are in good agreement with our observations.

All attempts to obtain single crystals of $Bi(N_3)_3$ by recrystallization or sublimation were unsuccessful because of the polymeric nature of $Bi(N_3)_3$. The identity of the bismuth triazide was established by the observed material balance, its vibrational spectra, and conversion into products that could be characterized by their crystal structures.

Neat $Bi(N_3)_3$ can explode violently upon provocation (e.g., scraping with a metal spatula, striking with a hammer, or

dx.doi.org/10.1021/ic202307a | *Inorg. Chem.* 2012, 51, 1127−1141

heating in an open flame). The sensitivity of $Bi(N_3)_3$ can be greatly reduced by either anion or adduct formation. The addition of ionic azides results in the formation of an anion, which increases the ionicity of the azido groups. The N_3^- anion possesses two double bonds, while a covalent N_3 group has a single and a triple bond. An increase of the ionicity of an azido ligand makes the breaking of an N−N bond more difficult and raises the activation energy barrier toward N_2 elimination. Thus, $[Bi(N_3)_4]^-$ and $[Bi(N_3)_5]^{2-}$ have been prepared by the reaction of neutral $Bi(N_3)_3$ with stoichiometric amounts of $A^+N_3^-$ (A = PPh_4, PNP) in acetonitrile (eqs 2 and 3). These anions can be handled more safely.

$$Bi(N_3)_3 + A^+N_3^- \xrightarrow{CH_3CN} [A^+][Bi(N_3)_4]^- \quad (2)$$

$$Bi(N_3)_3 + 2A^+N_3^- \xrightarrow{CH_3CN} [A^+]_2[Bi(N_3)_5]^{2-} \quad (3)$$

While the reaction of $Bi(N_3)_3$ with even a large excess of $PNPN_3$ (molar ratio 1:6) resulted in the formation of only the pentaazido anion $[Bi(N_3)_5]^{2-}$, a different result was obtained with PPh_4N_3 as the source of the ionic azide. The hexaazido bismuthite anion, $[Bi(N_3)_6]^{3-}$, was successfully obtained by the reaction of $Bi(N_3)_3$ with 3 equiv of PPh_4N_3 in acetonitrile (eq 4).

$$Bi(N_3)_3 + 3P(C_6H_5)_4N_3 \xrightarrow{CH_3CN} [P(C_6H_5)_4^+]_3[Bi(N_3)_6]^{3-} \quad (4)$$

All of these polyazido bismuthite salts were isolated as room-temperature-stable, crystalline solids of yellow to orange color. Because of the increased ionicity of their azido ligands and the presence of large counterions, which diminishes shock propagation, these compounds are much less sensitive and explosive than the parent compound, $Bi(N_3)_3$, and could be manipulated in our study at room temperature without explosion. The $[P(C_6H_5)_4]^+[Bi(N_3)_4]^-$ and $[P(C_6H_5)_4^+]_3[Bi(N_3)_6]^{3-}$ salts had also been described in an independent study,[23] and the reported properties agree well with those from our investigation.

$$Bi(N_3)_3 + 2bipy \rightarrow (bipy)_2 \cdot Bi(N_3)_3 \quad (5)$$

$$[P(C_6H_5)_4^+]_2[Bi(N_3)_5]^{2-} + bipy \rightarrow [P(C_6H_5)_4^+]_2[bipy \cdot Bi(N_3)_5]^{2-} \quad (6)$$

With CH_3CN solutions of 2,2′-bipyridine, the adducts $(bipy)_2 \cdot Bi(N_3)_3$ (eq 5) and $[P(C_6H_5)_4^+]_2[bipy \cdot Bi(N_3)_5]^{2-}$ (eq 6) were obtained. Although a seven-coordinated nitrogen-donor adduct of $Bi(N_3)_3$ with two pyridine molecules having a polymeric band structure has previously been reported,[24] the bis(2,2′-bipyridine) adduct has a highly unusual dimeric structure with a CN of 8.

Reactions of 2,2′-bipyridine were also carried out with $As(N_3)_3$ and $Sb(N_3)_3$ and resulted, even in the presence of a large excess of 2,2′-bipyridine, exclusively in the formation of stable 1:1 adducts (eqs 7 and 8), which were characterized by their crystal structures.

$$As(N_3)_3 + bipy \rightarrow bipy \cdot As(N_3)_3 \quad (7)$$

$$Sb(N_3)_3 + bipy \rightarrow bipy \cdot Sb(N_3)_3 \quad (8)$$

Attempts to prepare $Bi(N_3)_5$ were unsuccessful. Even at a temperature of −35 °C, the reaction of BiF_5 with an excess of Me_3SiN_3 in an acetonitrile solution resulted in the evolution of elemental nitrogen and the reduction of Bi(+V) to Bi(+III), yielding a pale-yellow precipitate of $Bi(N_3)_3$ (eq 9).

$$BiF_5 + 5Me_3SiN_3 \xrightarrow{CH_3CN} Bi(N_3)_3 + 3N_2 + 5Me_3SiF \quad (9)$$

Because the oxidation potential of an anion is lower than that of its neutral parent compound, $[P(C_6H_5)_4][BiF_6]$ was used as the starting material in an attempt to prepare a Bi(+V) azide. However, the reaction of $[P(C_6H_5)_4][BiF_6]$ with an excess of Me_3SiN_3 in an acetonitrile solution at −35 °C resulted again in the reduction of Bi(+V) to Bi(+III), yielding a yellow solution of $[P(C_6H_5)_4][Bi(N_3)_4]$.

Crystal Structures. Crystal structures were determined for $(bipy)_2 \cdot Bi(N_3)_3$, $bipy \cdot As(N_3)_3$, $bipy \cdot Sb(N_3)_3$, $[P(C_6H_5)_4][Bi(N_3)_4]$, $[PNP]_2[Bi(N_3)_5]$, $[P(C_6H_5)_4]_2[bipy \cdot Bi(N_3)_5]$, and $[P(C_6H_5)_4]_3[Bi(N_3)_6]$. Of these, the structures of $[P(C_6H_5)_4][Bi(N_3)_4]$ and $[P(C_6H_5)_4]_3[Bi(N_3)_6]$ have recently also been described by others.[23] While our structure of $[P(C_6H_5)_4][Bi(N_3)_4]$, which consists of polymeric chains of four-membered Bi_2N_2 rings (Figure 1), is in good agreement with the previous report,[23] the previously reported structure of $[P(C_6H_5)_4]_3[Bi(N_3)_6]$ appears to be flawed.

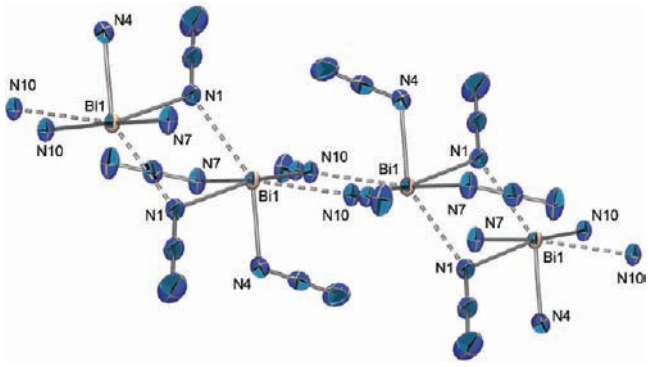

Figure 1. Chain structure of the $Bi(N_3)_4^-$ anion in $[P(C_6H_5)_4][Bi(N_3)_4]$. The bond distances and angles are very similar to those given in ref 23.

$[P(C_6H_5)_4][Bi(N_3)_4]$. The crystal structure of the $[P(C_6H_5)_4][Bi(N_3)_4]$ salt[37] shows the presence of polymeric anion chains (Figure 1) and isolated $[P(C_6H_5)_4]^+$ cations. The chains consist of planar four-membered Bi_2N_2 parallelograms resulting from two shorter and two longer Bi−N bonds. The planes of neighboring four-membered Bi_2N_2 parallelograms are rotated by 69° with respect to each other, while those of alternating rings are perfectly parallel to each other.

Although it has previously been stated[23] that the bismuth lone valence electron pair is sterically active, its exact location was not identified. The location of the bismuth lone valence electron pair can be deduced from the following analysis. The close environment around each bismuth atom consists of two terminal N_3 ligands, two $\mu^{1,1}$-bridging N_3 ligands, and the sterically active bismuth lone valence electron pair. This arrangement is derived from a pseudo-trigonal bipyramid with the two terminal N_3 ligands and the sterically active lone valence electron pair in the three equatorial positions

dx.doi.org/10.1021/ic202307a | Inorg. Chem. 2012, 51, 1127−1141

and the two bridging N_3 groups occupying the two axial positions (Figure 2).

Because of the increased repulsion from the sterically active lone pair, the axial N–Bi–N bond angle is compressed from the ideal 180° to 159.4°. The ligand arrangement in $[Bi(N_3)_4]^-$ resembles somewhat that of the monomeric $ESbN_4$ skeleton in $[N(CH_3)_4][Sb(N_3)_4]$, with one equatorial N_3 group pointing up and the other one pointing down and the two axial N_3 groups being tilted away from the lone pair. When the two long nitrogen bridges from the two neighboring $Bi(N_3)_4$ units are included in the coordination sphere, the CN of bismuth is increased to 7. In order to minimize the repulsion from the lone valence electron pair, the plane formed by the bridging nitrogen atoms and bismuth is tilted by 31.5° against the equatorial plane (Figure 2).

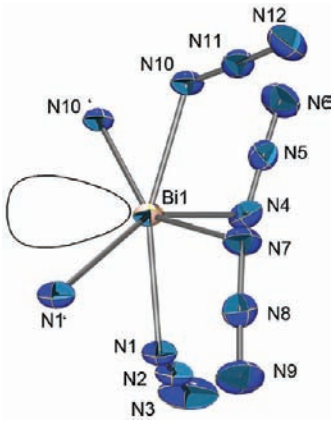

Figure 2. Structure of the isolated $Bi(N_3)_4^-$ unit, including the two bridging nitrogen atoms (N1′ and N10′) from two neighboring $Bi(N_3)_4^-$ units and showing the predicted location of the sterically active lone valence electron pair.

The two bridging N_3 ligands (N10–N11–N12) are coplanar with the corresponding four-membered rings (Figure 1). In addition, each bismuth atom possesses two terminal azido ligands (N4–N5–N6 and N7–N8–N9), which point in opposite directions and form an N–Bi–N angle of 80° due to compression from the bismuth lone valence electron pair. For a given Bi_2N_2 ring, the two azido ligands pointing toward each other (N4–N5–N6 and N7–N8–N9) are located above and below the ring.

[PNP]$_2$[Bi(N$_3$)$_5$]. This compound contains well-separated cations and monomeric anions.[38] The closest Bi···N and N···N contacts between neighboring anions are 8.8 and 7.4 Å, respectively. The skeleton of the $[Bi(N_3)_5]^{2-}$ anion (Figure 3) is a BiN_5E pseudo-octahedron where E represents a sterically active lone valence electron pair. The structure is analogous to those[39,40] of SF_5^-, SeF_5^-, TeF_5^-, ClF_5, BrF_5, and IF_5 and could be explained by the use of an sp hybrid of the central atom for the lone pair and the bonding of a mainly covalent, axial azido ligand [r_{Bi-N} = 2.195(9) Å] and of the two remaining p orbitals for the bonding of the four equatorial ligands by two linear, semiionic, 3c–4e bond pairs.[41] The semiionic, 3c–4e bonds result in more ionic ligands with an average r_{Bi-N} of 2.382 Å. Because of the increased repulsion from the more diffuse lone valence electron pair of bismuth, the equatorial nitrogen atoms are bent away from the lone pair and the equatorial N–Bi–N bond angles are compressed from the ideal 180° to 168°.

The structure of the closely related $[pyr]^+[Te(N_3)_5]^-$ salt has previously been reported.[7] Although the TeN_5 skeleton also has a pseudo-octahedral structure with one of the two axial positions occupied by a sterically active lone valence electron pair, the arrangement of the azido ligands in $[Bi(N_3)_5]^{2-}$ and $[Te(N_3)_5]^-$ differ substantially.

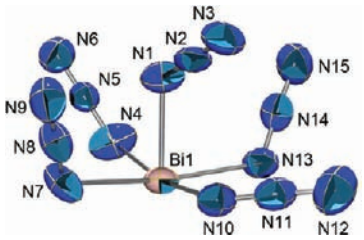

Figure 3. ORTEP plot for the anion in $[PNP]_2[Bi(N_3)_5]$. Thermal ellipsoids are shown at the 50% probability level. Selected bond lengths [Å] and angles [deg]: Bi1–N1 2.195(9), Bi1–N4 2.412(8), Bi1–N7 2.381(8), Bi1–N10 2.361(6), Bi1–N13 2.375(9), N1–N2 1.213(12), N2–N3 1.159(10), N4–N5 1.188(11), N5–N6 1.145(11), N7–N8 1.188(10), N8–N9 1.140(10), N10–N11 1.162(12), N11–N12 1.172(11), N13–N14 1.189(11), N14–N15 1.162(11); N1–Bi1–N10 87.0(3), N1–Bi1–N13 86.3(3), N10–Bi1–N13 88.0(4), N1–Bi1–N7 84.1(3), N10–Bi1–N7 83.5(3), N13–Bi1–N7 167.4(3), N1–Bi–N4 81.6(3), N10–Bi–N4 168.6(3), N13–Bi1–N4 90.6(3), N7–Bi–N4 96.0(3), Bi1–N1–N2 115.6(7), N1–N2–N3 176.4(10), Bi1–N4–N5, 127.6(7), N4–N5–N6 176.1(10), Bi1–N7–N8 117.5(6), N7–N8–N9 179.4(10), Bi1–N10–N11 125.4(7), N10–N11–N12 177.3(10), Bi1–N13–N14 120.1(6), N13–N14–N15 177.8(10).

In $[Te(N_3)_5]^-$, two equatorial ligands in the trans position point away from the lone pair, one points toward the lone pair, and the fourth one is located in the equatorial plane. In contrast, in $[Bi(N_3)_5]^{2-}$, three of the four equatorial azido ligands point away from the lone pair and the fourth one is forced by the axial azido ligand into the equatorial plane. The fact that in $[Bi(N_3)_5]^{2-}$ the axial azido group eclipses the equatorial Bi–N10 bond can be rationalized by the fact that the α-nitrogen of the axial azido group, N1, possesses two sterically active lone valence electron pairs that avoid eclipsing the other equatorial Bi–N bonds.

The structure of $[Te(N_3)_5]^-$ in $[pyr][Te(N_3)_5]$ is complicated by the fact that, because of the relatively small size of the pyridinium cation, the anions form an extended network.[7] Thus, each $[Te(N_3)_5]^-$ ion forms three long Te···N bridges of about 3.2 Å with three neighboring anions. The three bridging nitrogen atoms contact the anion in the axial position, which is occupied by the sterically active lone valence electron pair. Therefore, the close-range CN of tellurium is 6, but the large-range one is extended to 9 by the additional three very long nitrogen contacts.

[P(C$_6$H$_5$)$_4^+$]$_2$[bipy·Bi(N$_3$)$_5$]$^{2-}$. This compound also contains well-separated cations and monomeric anions.[42] The anion of this compound is depicted in Figure 4. In comparison to the lone $[Bi(N_3)_5]^{2-}$ anion, the sterically active lone valence electron pair on bismuth has been replaced by the bidentate 2,2′-bipyridine ligand. The perfect alignment of the bipyridine group with the axial Bi–N bond establishes that the lone valence electron pair on bismuth is no longer sterically active. Therefore, bismuth has a CN of 7 in this compound, and the structure of the $N_2BiN'_4N''$ skeleton represents a pseudo-monocapped trigonal prism, i.e., a 2:4:1 ligand arrangement, which is frequently encountered as a minimum-energy structure for CN 7.[16,43] One of the equatorial azido ligands, N10–N11–N12, showed unusual N_α–N_β and N_β–N_γ bond lengths and

dx.doi.org/10.1021/ic202307a | Inorg. Chem. 2012, 51, 1127–1141

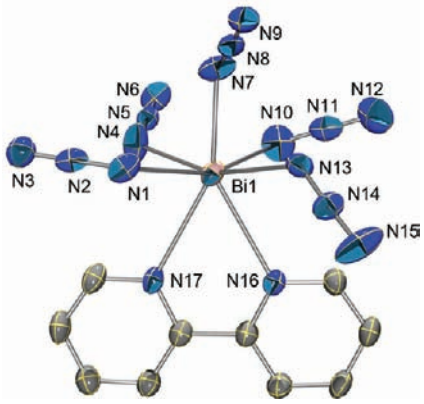

Figure 4. ORTEP plot for the anion in $[P(C_6H_5)_4]_2[bipy{\cdot}Bi(N_3)_5]$. Thermal ellipsoids are shown at the 50% probability level. Selected bond lengths [Å] and angles [deg]: Bi1–N1 2.539(3), Bi1–N4 2.366(4), Bi1–N7 2.314(4), Bi1–N10 2.387(5), Bi1–N13 2.448(3), Bi1–N16 2.834(3), Bi1–N17 2.820(3), N1–N2 1.190(5), N2–N3 1.163(5), N4–N5 1.189(4), N5–N6 1.150(4), N7–N8 1.207(5), N8–N9 1.154(5), N10–N11 1.177(9), N11–N12 1.169(8), N13–N14 1.179(5), N14–N15 1.155(5); N1–Bi1–N10 159.8(2), N1–Bi1–N13 93.35(11), N1–Bi1–N16 120.29(10), N10–Bi1–N13 88.9(2), N1–Bi1–N7 82.63(12), N10–Bi1–N7 79.0(2), N13–Bi1–N7 77.75(13), N1–Bi–N4 82.07(12), N10–Bi–N4 87.0(2), N13–Bi1–N4 159.21(14), N7–Bi–N4 81.46(15), N10–Bi–N17 111.7(2), N13–Bi1–N17 124.74(10), N1–Bi1–N17 81.91(10), N4–Bi1–N16 120.36(13), N4–Bi1–N17 75.51(12), N7–Bi1–N16 148.55(11), N10–Bi1–N16 79.9(2), N13–Bi1–N16 78.80(10), N7–Bi1–N17 153.76(12), N16–Bi1–N17 57.22(8), Bi1–N1–N2 119.3(3), N1–N2–N3 178.5(4), Bi1–N4–N5 120.4(3), N4–N5–N6 175.9(4), Bi1–N7–N8 119.8(3), N7–N8–N9 176.0(4), Bi1–N10–N11 116.3(4), N10–N11–N12 178.0(7), Bi1–N13–N14 129.9(3), N13–N14–N15 177.2(5).

large thermal parameters due to a 80:20 disorder. Refinement for the disorder resolved most of the problem, and the geometry shown in Figure 4 is that for the isomer with the 80% occupancy factor.

It is interesting to analyze the effect that the replacement of a lone valence electron pair by the bidentate 2,2′-bipyridine ligand has on the structure of the $Bi(N_3)_5$ group. Similar to the lone pair in the unsubstituted $[Bi(N_3)_5]^{2-}$ anion, the bulky 2,2′-bipyridine ligand is also more repulsive than the azido Bi–N bonds, causing the four equatorial Bi–N bonds to be bent toward the axial azido ligand. However, the arrangement of the azido ligands in the two anions is very different.

In $[Bi(N_3)_5]^{2-}$, three of the equatorial azido ligands point upward toward the axial azido ligand, while the fourth one is forced into the equatorial plane by the axial azido group. In $[bipy{\cdot}Bi(N_3)_5]^{2-}$, one of the equatorial azido groups points downward toward the 2,2′-bipyridine ligand, while the remaining three azido ligands are in the equatorial plane. In $[Bi(N_3)_5]^{2-}$, the axial azido group eclipses the Bi–N bond of the unique equatorial ligand, while in $[bipy{\cdot}Bi(N_3)_5]^{2-}$, its orientation is between the down-pointing and in-plane azido group. Although it is roughly perpendicular to the plane of the 2,2′-bipyridine ligand, it is closer to the down-pointing ligand, forming a dihedral angle of 160.8°. In both ions, the four skeletal equatorial nitrogen atoms are essentially coplanar, but the quadrangles are distorted from a square, with angles ranging from 82 to 96°. These distortions can be attributed to the directional effects of the axial azido groups, which increase some of the Bi–N bond lengths and N–Bi–N bond angles. Because of the steric inactivity of the lone valence electron pair of bismuth in $[bipy{\cdot}Bi(N_3)_5]^{2-}$, the Bi–N bond lengths of its $Bi(N_3)_5$ group no longer exhibit the trends generally observed[44] for a hypervalent EAX4X′-type species, such as $[Bi(N_3)_5]^{2-}$. Instead, they appear to be governed by the directional repulsion effects of the axial azido ligand, causing a lengthening of the two equatorial Bi–N bonds pointing in the same direction.

$[P(C_6H_5)_4]_3[Bi(N_3)_6]$. The crystal structure of this compound has been determined independently in our laboratory[45] and at the University of Rostock, Rostock, Germany.[23] The two sets of crystallographic data are in good general agreement, but both structures suffer from varying degrees of disorder, complicating the refinements. The Rostock group has reported very unusual bond distances of Bi–N16 = 2.719 Å and N17–N18 = 1.19 Å for the N16–N17–N18 azido ligand.[23] These large deviations from the normal range of Bi–N distances are unexpected even for a disordered azido group but are similar to cases where an azido position is partially replaced by a chlorido ligand. Because the Rostock group recrystallized their compound from CH_2Cl_2 and because the use of chlorinated solvents can lead to an azido–chlorido back-exchange,[46] the Rostock crystal may have been contaminated by chloride. The explanation given by the Rostock authors that the very long Bi–N16 distance might be due to a bridging azido ligand is unlikely because the anions in $[P(C_6H_5)_4]_3[Bi(N_3)_6]$ are very well separated from each other (Figure 5).

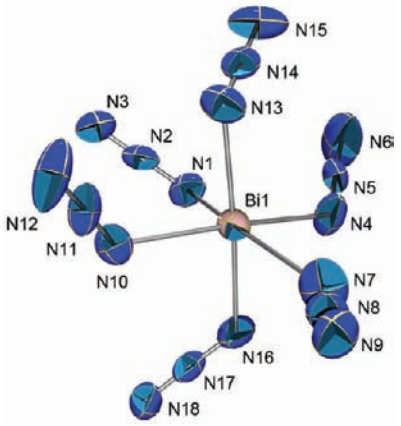

Figure 5. ORTEP plot for the anion in $[P(C_6H_5)_4]_3[Bi(N_3)_6]$. Thermal ellipsoids are shown at the 50% probability level. Selected bond lengths [Å] and angles [deg]: Bi1–N1 2.339(4), Bi1–N4 2.371(4), Bi1–N7 2.566(6), Bi1–N10 2.476(4), Bi1–N13 2.482(4), Bi1–N16 2.356(4), N1–N2 1.197(5), N2–N3 1.158(5), N4–N5 1.137(5), N5–N6 1.128(6), N7–N8 1.165(5), N8–N9 1.149(6), N10–N11 1.186(5), N11–N12 1.165(5), N13–N14 1.179(5), N14–N15 1.160(5), N16–N17 1.202(5), N17–N18 1.142(5); N1–Bi1–N10 84.53(12), N1–Bi1–N13 85.68(13), N1–Bi1–N16 89.55(14), N10–Bi1–N13 88.99(13), N1–Bi1–N7 177.5(2), N10–Bi1–N7 96.6(3), N13–Bi1–N7 92.1(2), N1–Bi–N4 82.41(14), N10–Bi–N4 164.45(14), N13–Bi1–N4 93.38(14), N7–Bi–N4 96.7(3), N4–Bi1–N16 82.60(16), N7–Bi1–N16 92.7(2), N10–Bi1–N16 88.91(14), N13–Bi1–N16 174.96(14), Bi1–N1–N2 119.1(3), N1–N2–N3 177.2(5), Bi1–N4–N5 122.5(3), N4–N5–N6 177.1(6), Bi1–N7–N8 137.2(5), N7–N8–N9 172.4(8), Bi1–N10–N11 120.8(3), N10–N11–N12 177.7(5), Bi1–N13–N14 119.4(3), N13–N14–N15 176.5(5), Bi1–N16–N17 124.0(3), N16–N17–N18 177.5(4).

The previous description[23] of the $[Bi(N_3)_6]^{3-}$ structure is also flawed. On the one hand, the Rostock authors state that the lone valence electron pair on bismuth is sterically active, but

dx.doi.org/10.1021/ic202307a | Inorg. Chem. 2012, 51, 1127–1141

in the next sentence, they say that, on the basis of the results from their NBO analysis of their DFT calculations, the lone pair has 99.5% s character. Arguably, this should render it sterically inactive. Unfortunately, NBO analysis is unsuitable for analysis of high CN (hypervalent) structures because such moleculesdo not conform to Pauling's classical theory of valence-shell orbital hybridization. For example, our own NBO calculations on $[Bi(N_3)_6]^{3-}$ showed the presence of 7.5 non-Lewis electrons and completely failed to account for three of the six Bi−N bonds. Furthermore, the lone pair on bismuth was calculated to be of 98% s character, which again is unrealistic because of the observed strong steric activity of the lone valence electron pair.

Furthermore, the Rostock authors state that the structure of the BiN_6 skeleton is strongly distorted and that its structure is best compared to that of $[Te(N_3)_6]^{2-}$.[8] However, the structure of $[Te(N_3)_6]^{2-}$ is derived from a pseudo-pentagonal bipyramid in which the lone valence electron pair occupies one of the five equatorial positions, whereas that of $[Bi(N_3)_6]^{3-}$ is best described as a monocapped octahedron in which the lone pair serves as the cap. This conclusion is based on the observation of three shorter and three longer Bi−N bonds and a compression of the cone angle formed by the shorter bonds and a widening of that formed by the longer bonds. These features are characteristic for a monocapped octahedron in which the lone valence electron pair is located in the center of the triangular face having the larger cone angle, as found for IF_6^-.[33]

$Bi(N_3)_3$. Because our attempts to grow single crystals of $Bi(N_3)_3$ were unsuccessful, its powder X-ray diffraction pattern was recorded at room temperature and compared to that calculated for $Sb(N_3)_3$ from the published single-crystal structure data obtained at 223 K.[9] The two data sets were very different, ruling out the possibility that $Bi(N_3)_3$ at room temperature is isostructural with $Sb(N_3)_3$ at 223 K. The experimental powder X-ray diffraction pattern of $Bi(N_3)_3$ and the one calculated for $Sb(N_3)_3$ are given in the Supporting Information.

bipy·$M(N_3)_3$ (M = As, Sb). These two compounds are isostructural[47,48] and contain relatively well-isolated monomeric bipy·$M(N_3)_3$ molecules. Thus, each bipy·$Sb(N_3)_3$ molecule has only two Sb−N contacts of 3.41 and 3.33 Å with two neighbors that are shorter than the sum of the van der Waals radii of antimony and nitrogen (3.58 Å).[49]

The structure might be considered either as a very strongly distorted pseudo-octahedron with the two axial positions occupied by the nitrogen with the shortest Sb−N bond (2.078 Å) and the sterically active lone valence electron pair E of antimony (Figure 6) or as derived from a distorted pseudo-tetrahedral $ESb(N_3)_3$ molecule that is connected sideways to a more weakly bonded 2,2′-bipyridine ligand with Sb−N bonds of ∼2.55 Å (Figure 7). We prefer the latter description. It moves the lone valence electron pair E away from the axis of the octahedron and closer to a pseudo-C_3 axis of a distorted EMN_3 tetrahedron. This can account for the observed strong distortions from an ideal pseudo-octahedral arrangement. The structure of bipy·$As(N_3)_3$ is analogous, and its details are given in the Supporting Information.

[(bipy)$_2$·$Bi(N_3)_3$]$_2$. The crystal structure of $[(bipy)_2{\cdot}Bi(N_3)_3]$ consists of well-separated dimers.[47] The presence of four bulky 2,2′-bipyridine groups in each dimer prevents any further association of the bismuth atoms through Bi−N bridges. The structure of the dimeric unit is shown in Figure 8.

The central part of this molecule is a four-membered Bi_2N_2 parallelogram with two $\mu^{1,1}$-bridging N_3 groups with a Bi−N bond distance of 2.510(3) Å. In addition, each bismuth atom possesses two terminal azido ligands with shorter Bi−N bonds of 2.345(4) and 2.438 Å, respectively. The coordination sphere around each bismuth atom is completed by four nitrogen atoms from two 2,2′-bipyridine ligands with three Bi−N bonds of about 2.59 Å and a longer one of 2.72 Å. The high symmetry (C_i) of the overall structure and lack of distortion show that the lone valence electron pair of bismuth is sterically inactive, thus giving each bismuth a CN of 8.

The energetically most favorable structure for CN 8 is a square antiprism,[50−53] and this arrangement is also found in this case.

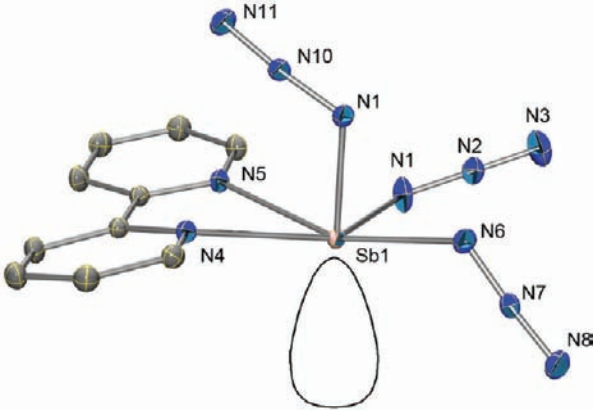

Figure 6. ORTEP plot of bipy·$Sb(N_3)_3$. The lone valence electron pair of antimony is assumed to be located in an axial position of a distorted pseudo-octahedron as shown. Thermal ellipsoids are shown at the 50% probability level. Selected bond lengths [Å] and angles [deg]: Sb1−N1 2.1495(10), Sb1−N4 2.6011(9), Sb1−N5 2.4858(9), Sb1−N6 2.2127(10), Sb1−N9 2.0783(9), N1−N2 1.2162(14), N2−N3 1.1418(15), N4−C1 1.3388(14), N4−C5 1.3479(13), N5−C7 1.3450(14), N5−C6 1.3559(14), N6−N7 1.2049(13), N7−N8 1.1543(14), N9−N10 1.2195(13), N10−N11 1.1400(14); N1−Sb1−N9 89.84(4), N1−Sb1−N6 85.96(4), N1−Sb1−N5 81.19(4), N1−Sb1−N4 143.86(4), N6−Sb1−N4 124.06(3), N9−Sb1−N6 77.39(4), N5−Sb1−N9 84.87(3), N5−Sb1−N6 158.09(3), N9−Sb1−N4 79.30(3), N5−Sb1−N4 63.69(3), Sb1−N1−N2 119.14(8), N1−N2−N3 176.14(13), Sb1−N6−N7, 121.80(8), N6−N7−N8 175.86(11), Sb1−N9−N10 118.68(7), N9−N10−N11 175.10(11).

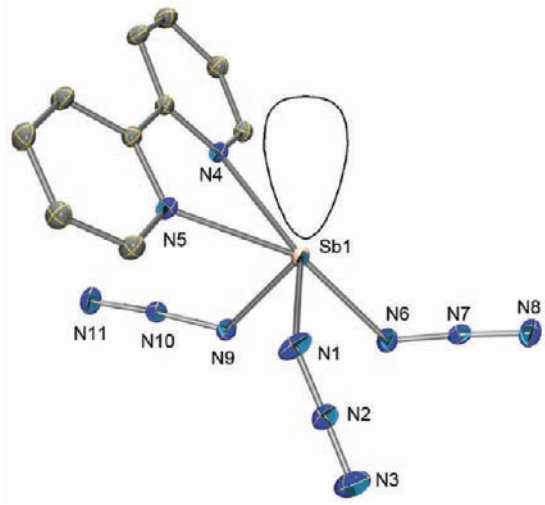

Figure 7. Alternate location of the sterically active lone valence electron pair in bipy·$Sb(N_3)_3$. The lone pair is located on a pseudo-C_3 axis of a ESb1N1N6N9 tetrahedron and avoids the two long Sb---N contacts from two neighbors.

dx.doi.org/10.1021/ic202307a | *Inorg. Chem.* 2012, 51, 1127−1141

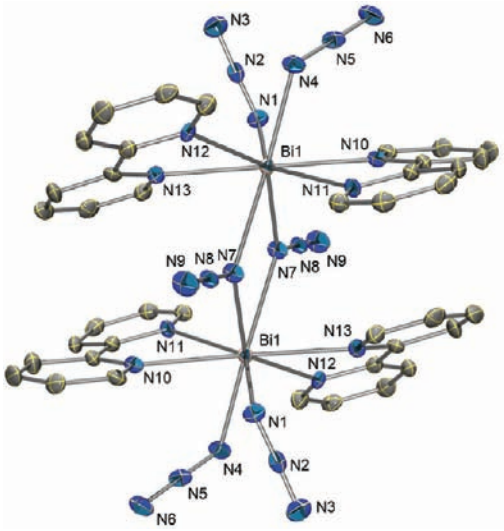

Figure 8. ORTEP plot of $[(bipy)_2{\cdot}Bi(N_3)_3]_2$. Thermal ellipsoids are shown at the 50% probability level. The bond lengths and angles are given in the Supporting Information.

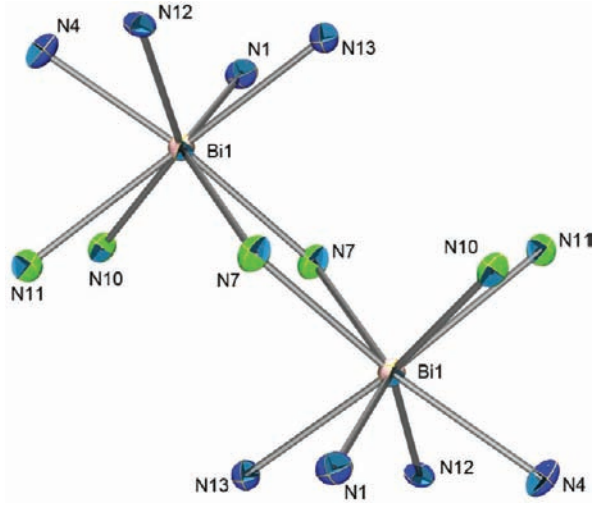

Figure 9. ORTEP plot of the skeleton of $[(bipy)_2{\cdot}Bi(N_3)_3]_2$. Thermal ellipsoids are shown at the 50% probability level. The atoms shown in green are coplanar, as are those in blue, and their planes are almost parallel with a tilt angle of only 6.9°. N7–N7–N10–N11 and N1–N4–N12–N13 do not form perfect squares with N7–N7 = 2.853 Å, N10–N11 = 2.733 Å, N7–N11 = 3.325 Å, N7–N10 = 3.229 Å, N1–N4 = 3.086 Å, N1–N13 = 3.053 Å, N4–N12 = 2.986 Å, and N12–N13 = 2.676 Å. The N1 and N4 atoms belong to the two terminal azido ligands, and the azido bridges are asymmetric. Selected bond lengths [Å] and angles [deg]: Bi1–N1 2.345(4), Bi1–N4 2.438(3), Bi1–N7 2.510(3), Bi1–N7′ 2.693(3), Bi1–N10 2.584(3), Bi1–N11 2.723(3), Bi1–N12 2.611(3), Bi1–N13 2.587(3), N1–N2 1.197(5), N2–N3 1.167(5), N4–N5 1.202(5), N5–N6 1.151(5), N7–N8 1.208(5), N8–N9 1.145(5); N1–Bi1–N4 80.34(12), N1–Bi1–N7 80.03(12), N1–Bi1–N13 76.30(11), N4–Bi1–N12 72.41(11), N7–Bi1–N10 78.63(11), N12–Bi1–N13 61.96(10), N7–Bi1–N7′ 66.39(13), N11–Bi1–N10 61.91(10), N7′–Bi1–N12 77.81(10), N7′–Bi1–N11 75.75(10), N4–Bi1–N11 77.78(11), N4–Bi1–N10 78.65(11), N12–Bi1–N11 89.64(10), N7–Bi1–N13 84.58(11), N7′–Bi1–N13 75.54(10), N1–Bi1–N10 80,86(12), Bi1–N1–N2 116.4(3), N1–N2–N3 177.7(5), Bi1–N4–N5 119.6(3), Bi1–N7–N8 124.1 (3), Bi1–N7–Bi1′ 113.60(13).

Hence, the structure of the skeleton of the dimer (Figure 9) is best described as two pseudo-square antiprisms sharing a common edge consisting of the two N_α atoms of the bridging azido groups. This structural type is rather unique and, to our best knowledge, has not been observed before in any other polyazide.

Vibrational Spectra. Vibrational spectroscopy, in particular, Raman spectroscopy, is a powerful tool for the characterization of polyazides. The spectra not only establish the presence of the azido ligands but also demonstrate the completeness of the halo–azido ligand-exchange reactions and the purity of the resulting materials. Although the spectra of the skeletons can be very similar, the antisymmetric stretching bands of the azido groups are strongly influenced by their orientation and, therefore, can provide much useful information. These bands occur in a range that is not obscured by solvent or cation bands, and their frequencies, splittings, and particularly their relative intensities vary considerably from compound to compound. Thus, the knowledge of both the crystal structures and Raman spectra allows the correlation of certain Raman patterns with specific azido ligand arrangements. In the absence of crystal structures, the observed Raman spectra can be analyzed by a comparison with those predicted by quantum-chemical (QC) calculations for different isomers and, hence, might allow a choice between them.

Because the frequency differences between the antisymmetric N_3 stretching mode (or more accurately the N≡N stretching mode) of a $\mu^{1,1}$-bridging N_3 group and a nonbridging terminal one are quite small, the bands cannot be easily assigned to the individual groups based on their frequencies alone but can be distinguished based on the observed relative intensities and splittings. This point is demonstrated by the Raman spectra of $Sb(N_3)_3$ and $As(N_3)_3$.[9] The antimony compound contains only three identical $\mu^{1,1}$-bridging N_3 groups, forming a three-ring "Mitsubishi"-type pattern. Its Raman spectrum is very clean and shows only the predicted two Raman bands, the in-phase coupled mode at 2123 cm^{-1} and the out of-phase coupled mode at 2079 cm^{-1}. In contrast, the arsenic compound contains two $\mu^{1,1}$-bridging N_3 groups and one nonbridging azido ligand. Accordingly, the Raman spectrum shows three Raman bands at 2128, 2103, and 2093 cm^{-1}, respectively. Their frequencies are too similar for firm assignments, although by comparison with those of $Sb(N_3)_3$, the 2128 and 2093 cm^{-1} bands most likely belong to the $\mu^{1,1}$-bridging N_3 groups.

Raman spectra were recorded for all of the compounds of this study and demonstrate the presence of predominantly covalent azido ligands. Their frequencies are listed in the Experimental Section and were confirmed by QC calculations. As shown in Figure 10, increasing the negative charge on the molecule leads to an increase in the ionicity of the azido ligands and results in the expected shift to lower frequencies.

Structural Motifs for the Binary Group 15 Polyazides. *General Aspects.* As a general rule, arsenic, antimony, and bismuth seek, whenever possible, to attain high CNs.[39] This goal can be achieved by the association and/or addition of more azide ligands, leading to the formation of anions. The tendency for the association of anions can be suppressed by the use of large cations, which favors the formation of isolated monomeric anions, as found for $[PNP]_2[Bi(N_3)_5]$ and $[P(C_6H_5)_4]_3[Bi(N_3)_6]$. With tightly bound ligands, such as fluoride, arsenic generally has a maximum CN of 6 (see AsF_6^-), whereas antimony and bismuth can have higher CNs and form, for example, stable $[MF_7]^{2-}$ anions.[54] With loosely bound ligands and longer bonds, such as bridging atoms, even higher CNs are possible, and arsenic can also have CN 7.[9] In general,

dx.doi.org/10.1021/ic202307a | Inorg. Chem. 2012, 51, 1127–1141

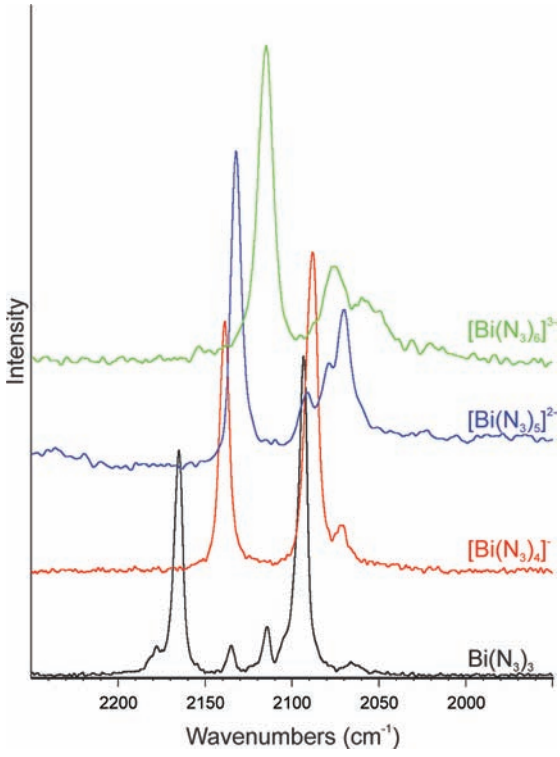

Figure 10. Antisymmetric N_3 stretching modes (ν_{as} N_3) of $[Bi(N_3)_{3+n}]^{n-}$ in the Raman spectra of $Bi(N_3)_3$, $[P(C_6H_5)_4][Bi(N_3)_4]$, $[PNP]_2[Bi(N_3)_5]$, and $[P(C_6H_5)_4]_3[Bi(N_3)_6]$.

CNs of 4, 6, and 8 are energetically more favorable, but this does not preclude those of 5 and 7.

A further complexity occurs for the pnictogen(+III) compounds because of the presence of a lone valence electron pair. In numerous cases, this lone pair can become sterically active and, thus, contribute to the overall coordination.

A common building block for the association of polyazides is the formation of four-membered M_2N_2 rings involving $\mu^{1,1}$-bridging N_3 groups. Because the two original M−N_3 bonds are shorter than the two M···N_3 bridge bonds, the rings have the shape of a parallelogram. For extension of the CN of M by 1, only one such ring is required resulting in a dimeric species. A typical example of such a structure is $[(N_3)_2Ga(CH_2)_3NMe_2]$ (Figure 11).[55]

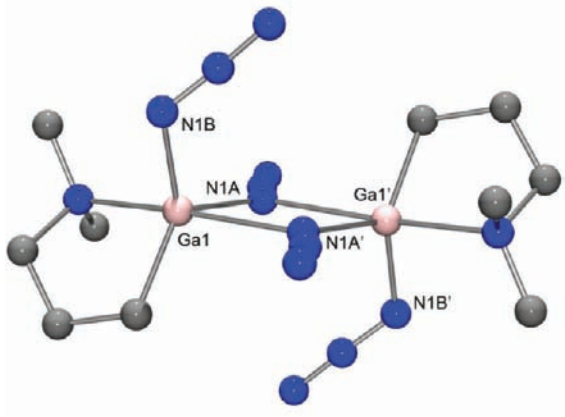

Figure 11. Crystal structure of $[(N_3)_2Ga(CH_2)_3NMe_2]$ from ref 55, showing a single M_2N_2 parallelogram with $\mu^{1,1}$-bridging N_3 groups. The two terminal azido groups point toward the ring.

For an extension of the CN by 2, each M atom can form two such rings, resulting in polymeric band structures, as found for $[Bi(N_3)_4]^-$ (Figure 1). The CN of M in these band structures can be further extended by 1 either by an additional $\mu^{1,3}$-bridging N_3 group between the bands, as in $As(N_3)_3$,[9] or by M forming a third M_2N_2 ring, resulting in the formation of a polymeric sheet structure, as in $Sb(N_3)_3$ (Figure 12).[9]

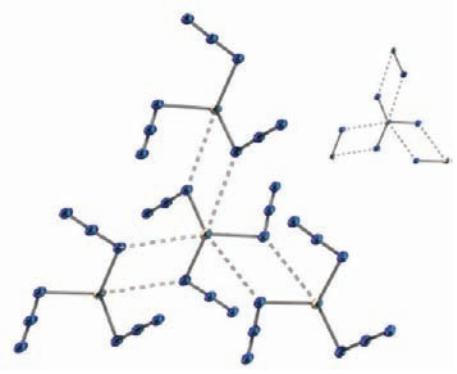

Figure 12. Polymeric sheet structure of $Sb(N_3)_3$ from ref 9, showing the triple M_2N_2 parallelograms with $\mu^{1,1}$-bridging N_3 groups. The inset shows the "Mitsubishi" emblem.

Because the three parallelograms in the sheet structure are derived from a pyramidal MN_3 backbone, they are not coplanar but form angles of about 77° with each other, resulting in an arrangement closely resembling the "Mitsubishi emblem".[9] For the arrangement in the band structure where a central atom forms only two of these parallelograms, the term "half-Mitsubishi" has been coined.[9] Another method for extension of the CN of M can be achieved by the use of one or more donor ligands, such as pyridine[24] or 2,2′-bipyridine,[22] as is also demonstrated in the current study.

Another interesting aspect of these polyazide compounds is the floppiness of the azido ligands, resulting in highly fluxional structures. Most of the time, the energy differences between structural isomers are so small that minor changes in the packing energies can result in different arrangements of the azido ligands. This raises the question about the true minimum-energy structures of these species. Solid-state effects can be avoided by obtaining solution data, but solvent effects can also influence the structures, and it is therefore important to use different solvents to study this effect. A potential approach is the use of QC calculations on the free molecular species, but care has to be taken with the chosen computational method because different minimum-energy structures can be found that are dependent on the method used. In addition, one has to be careful about the structure of highly charged negative ions, which may not support all bound electrons. Thus, the calculations for the free gaseous species should be performed at the highest possible level in terms of the treatment of the *n*-particle effects (correlation energy) and the 1-particle effects (the basis set), especially when an experimental structure of the free molecule is not available. All of these issues can make the choice of the preferred geometry of the isolated molecular structure difficult. Should one use the global minimum from a high-level calculation for the free gaseous species, the experimental structure from the solid, which could be influenced by solid-state effects, or solution data, which could be affected by solvent effects?

dx.doi.org/10.1021/ic202307a | *Inorg. Chem.* 2012, 51, 1127−1141

[Bi(N$_3$)$_4$]$^-$. As noted above, bismuth prefers CNs larger than 5. This can be accomplished by the formation of a "half-Mitsubishi" polymeric band structure, where each bismuth atom forms two of these parallelograms (Figure 1), giving bismuth a CN of 7 (Figure 2) in the solid state.

[Bi(N$_3$)$_5$]$^{2-}$. This anion with five azido ligands and one sterically active lone valence electron pair already has an innate CN of 6 and, therefore, does not associate any further in its PNP^+ salt. The influence of the cation size on the anion structure is nicely demonstrated by the structure found for the analogous $[Te(N_3)_5]^-$ anion in its pyridinium salt.[7] With one sterically active tellurium lone valence electron pair, $[Te(N_3)_5]^-$ also has CN 6. However, because of the presence of only one much smaller cation, the $[Te(N_3)_5]^-$ anion associates further, forming a polymeric anion network with three very long Te···N bridges, which, when included in the total coordination, result in CN 9 for tellurium.

[bipy·Bi(N$_3$)$_5$]$^{2-}$. When the CN of bismuth in $[Bi(N_3)_5]^{2-}$ is increased through the addition of one bidentate 2,2′-bipyridine ligand with two relatively short Bi−N bonds, the lone valence pair on bismuth becomes sterically inactive, giving bismuth CN 7 (Figure 4). This demonstrates that the CN of bismuth with tightly bound ligands is limited to 7 in the solid state, in accordance with our previous findings for bismuth fluorides.[54]

[Bi(N$_3$)$_6$]$^{3-}$. For arsenic and antimony, the V+ anions, $[As(N_3)_6]^-$ and $[Sb(N_3)_6]^-$, are well-known and, in the absence of a lone valence electron pair on M, have S_6 structures with octahedral MN_6 skeletons. Although our attempts to prepare the analogous $[Bi(N_3)_6]^-$ anion failed because of the high oxidizing power of bismuth(+V), the bismuth(+III) trianion $[Bi(N_3)_6]^{3-}$ could be prepared. Because bismuth can accommodate seven ligands without a problem,[51] the lone valence electron pair in $[Bi(N_3)_6]^{3-}$ is sterically active. It occupies the center of one triangular face of a pseudo-octahedron (Figure 13), so that the cone angle of

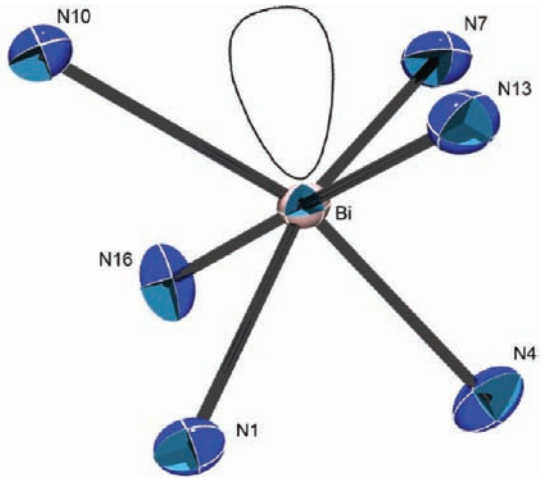

Figure 13. BiN_6 skeleton of $[Bi(N_3)_6]^{3-}$ showing the location of the sterically active lone valence electron pair of bismuth.

the face containing the lone valence pair is expanded and the cone angle of the corresponding opposite face is compressed.

The resulting monocapped octahedral structure of the skeleton is very different from that in the closely related $[Te(N_3)_6]^{2-}$ dianion, which is a pseudo-pentagonal bipyramid.[8] In both cases, the countercations, $[P(C_6H_5)_4]^+$, are identical, serving as a further example of how changes of the central atom and the formal charge can influence the arrangement of the azido ligands.

M(N$_3$)$_3$ (M = As, Sb, Bi). The structures of $As(N_3)_3$ and $Sb(N_3)_3$ have previously been described.[9] The structure of $As(N_3)_3$ can be described as a polymeric "half-Mitsubishi" band structure with an additional N_γ bridge from a neighboring band and a sterically active lone valence electron pair, resulting in a CN 7 monocapped octahedron with three short As−N bonds, three long As···N bridges, and the lone valence electron pair located in the center of the N1′−N4′−N6′ triangle formed by the three bridges (Figure 14). The structure of $Sb(N_3)_3$ is a

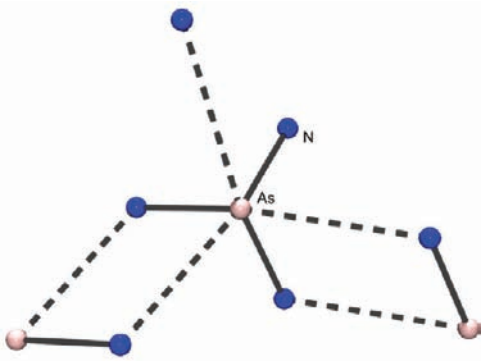

Figure 14. Polymeric band structure of $As(N_3)_3$ from ref 9, showing the two M_2N_2 parallelograms with $\mu^{1,1}$-bridging N_3 groups, one terminal nonbridging azido group nitrogen (N7) and one long nitrogen bridge (N6′) from a neighboring $As(N_3)_3$ unit.

polymeric "full Mitsubishi" sheet structure, again with a CN 7 monocapped octahedron possessing three short Sb−N bonds and three long Sb···N bridges, with the lone electron pair being located in the center of the triangle formed by the long bridges. The only difference compared to the solid-state structure of $As(N_3)_3$ is that all three Sb···N bridges are identical and originate from $Sb(N_3)_3$ units within the same sheet (Figure 12).

It is not unreasonable to predict that the solid-state structure of $Bi(N_3)_3$ would have a similar polymeric structure with CN 7 or higher. Unfortunately, the high shock sensitivity and the low solubility of $Bi(N_3)_3$ have prevented the growth of single crystals. However, its room-temperature powder X-ray diffraction pattern was recorded and shown to be different from that calculated for $Sb(N_3)_3$ from the published 223 K single-crystal structure,[9] and it is quite possible that, in the solid state, $Bi(N_3)_3$ is more strongly associated than both $As(N_3)_3$ and $Sb(N_3)_3$.

bipy·M(N$_3$)$_3$ (M = As, Sb). Another approach toward increasing the CNs of M in $M(N_3)_3$ is by complex formation with a nitrogen-donor ligand. Using one molecule of the bidentate 2,2′-bipyridine as a donor, the basic CN of $EM(N_3)_3$ can be increased from 4 to 6. Interestingly, the resulting $EMN_3N'_2$ skeletons deviate very strongly from pseudo-octahedral geometry and more closely approximate that of an EMN_3 pseudo-tetrahedron, with the two additional longer M−N′ bonds being located at an angle to the C_3 axis of the tetrahedron (Figure 7).

[(bipy)$_2$·Bi(N$_3$)$_3$]$_2$. Because bismuth prefers higher CNs, it is not surprising that $Bi(N_3)_3$ not only adds a second molecule of 2,2′-bipyridine but also dimerizes through the formation of one Bi_2N_2 parallelogram. This results in a CN of 8 at the bismuth atom and renders the lone valence electron pair of bismuth sterically inactive. Generally, the energetically most favorable arrangement for eight ligands is a square antiprism,[51−53] and this is also found for $[(bipy)_2{\cdot}Bi(N_3)_3]_2$. In this dimer, the two square antiprisms are coupled through a Bi_2N_2 parallelogram (Figure 9).

dx.doi.org/10.1021/ic202307a | Inorg. Chem. 2012, 51, 1127−1141

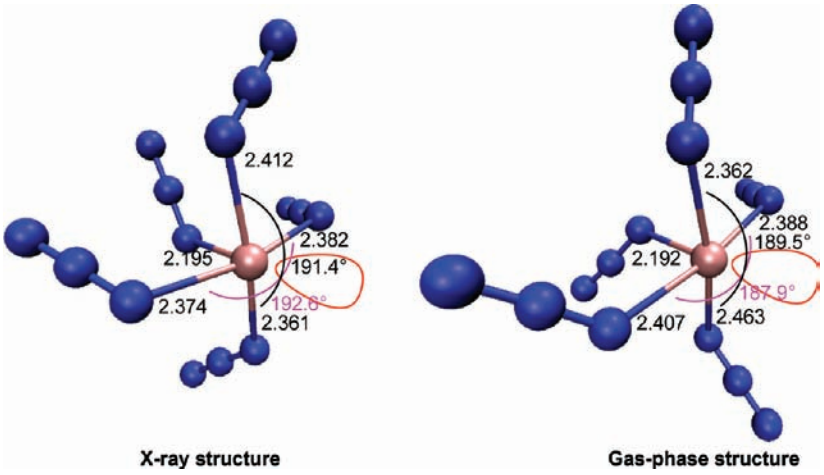

Figure 15. Solid-state $[PNP^+]_2$ salt and gas-phase structures of the $[Bi(N_3)_5]^{2-}$ anion. The depicted angles are N−Bi−N bond angles; bond lengths are given in angstrom.

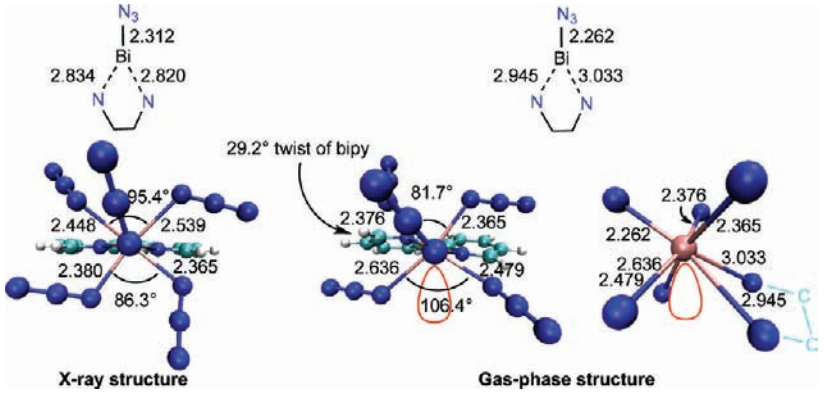

Figure 16. Structure of free gaseous $[bipy{\cdot}Bi(N_3)_5]^{2-}$ is markedly different from the experimentally determined solid $[P(C_6H_5)_4^+]_2$ salt, indicating steric inactivity and activity of the lone valence bismuth electron pair (red) in the solid state and gas phase, respectively. The given angles are N−Bi−N bond angles. It should be noted that the projection of the skeleton at the right has been rotated by 45° relative to the other two projections, which show an axial view of the 1:4:2 arrangement, analogous to that of Figure 4, to better reflect the 1:4:3 ligand arrangement in the free ion.

COMPUTATIONAL RESULTS

In order to estimate the influences of structural lattice and solvation effects, gas-phase DFT M06-2X calculations on the free species were performed with large basis sets. For the accurate prediction of unperturbed "true" conformations and energies of each species, their entire conformational space would need to be explored. Because of the low-barrier torsions about the M−N bonds, this has not been done. Instead, our starting structures have been the experimentally determined crystal structure conformations. Therefore, the presented structural deviation from the experiment should be taken as a measure of the crystal lattice effect on the considered conformer. The following results were obtained for $[Bi(N_3)_5]^{2-}$, $[bipy{\cdot}Bi(N_3)_5]^{2-}$, $[(bipy)_2{\cdot}Bi(N_3)_3]_2$, and $[Bi(N_3)_6]^{3-}$.

$[Bi(N_3)_5]^{2-}$. Both the gas-phase and solid-state structures of the pseudo-octahedral $[Bi(N_3)_5]^{2-}$ ion show the presence of a sterically active lone valence electron pair. The main difference between the two structures is the rotation of the axial and two opposing equatorial azido ligands. These rotations occurred during the optimization procedure of the gas-phase structure because of a very flat PES. As a consequence, the Bi−N bond distances for three azido ligands changed by as much as 0.10 Å, while all of the other bond lengths and angles remained close to their solid-state values (Figure 15).

$[bipy{\cdot}Bi(N_3)_5]^{2-}$. As mentioned earlier, the addition of a chelating 2,2′-bipyridine ligand to $[Bi(N_3)_5]^{2-}$ deactivates its otherwise sterically active lone valence electron pair in the solid state. In the resulting pseudo-monocapped trigonal prism (2:4:1 arrangement; see Figure 4), the opening of one equatorial N−Bi−N angle to 95.4° and the compression of the opposing one to 86.3° can be attributed to the repulsive effect of the axial azido ligand. Interestingly, our calculations show that, for gaseous $[bipy{\cdot}Bi(N_3)_5]^{2-}$, the lone valence electron pair becomes sterically active, resulting in large deviations from the experimental solid-state structure (Figure 16). Thus, in the free gaseous ion, the lengths of the bipyridine Bi−N bonds show a substantial increase ranging from 0.1 to 0.2 Å, their N−C−C−N twist angle is increased from 1.4° to 29.2°, and the formerly equatorial N−Bi−N angle of 86.3° increases to 106.4°, while the formerly larger N−Bi−N angle of 95.4° is compressed to 81.7°.

These changes indicate that the lone valence electron pair of bismuth occupies the face of a quadrangular cone formed by two azido groups and the 2.2′-bipyridine ligand, opening up their cone angle and lengthening their Bi−N bonds while compressing the opposite triangular cone and shortening the Bi−N bonds. Therefore, the structure of the free gaseous $[bipy{\cdot}Bi(N_3)_5]^{2-}$ anion can be described as a highly unusual eight-coordinated 1:4:3 arrangement (far right structure in Figure 16). It is derived from a pseudo-monocapped octahedron in which the lone pair is located in the cap, and the capped triangular face has been replaced by a rectangle because of substitution of an azido ligand by a bidentate bipyridine ligand.

In an effort to elucidate solvation effects on the structure of the free gaseous ion, we also optimized the geometry of the $[bipy{\cdot}Bi(N_3)_5]^{2-}$ anion in the PCM approximation with acetonitrile as the solvent. In this approximation, the lone valence electron pair of bismuth is

dx.doi.org/10.1021/ic202307a | Inorg. Chem. 2012, 51, 1127−1141

predicted to be sterically active (Figure 17), but its activity is less pronounced than that in the free ion (Figure 16).

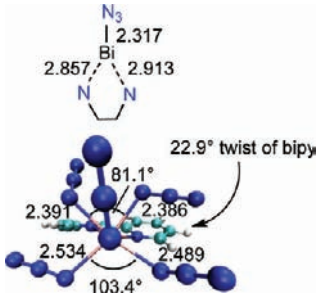

Figure 17. Optimization of the $[bipy{\cdot}Bi(N_3)_5]^{2-}$ anion in an acetonitrile solution predicting a geometry more similar to that of the free anion, i.e., a pronounced steric activity of the lone valence electron pair. The given angles are N–Bi–N.

The reduction in the steric activity of the lone valence electron pair in a chemical environment, such as positively charged counterions or polar solvents, can be attributed to the transfer of some electron density from the central atom to the ligands, thereby reducing the repulsion experienced by the lone pair in the center of the molecule and increasing the repulsion by the more negatively charged ligands. This increases the probability that the lone valence electron pair will reside on the central atom and become sterically inactive.

$[Bi(N_3)_6]^{3-}$. A triply charged anion in the gas phase typically requires very large basis sets for a proper treatment of its diffuse outer electrons. In the case of $[Bi(N_3)_6]^{3-}$, the applied cc-pwCVTZ-PP basis set on bismuth and cc-pVTZ basis set on nitrogen resulted in some electrons being slightly unbound (positive eigenvalues in the closed-shell singlet). This could be indicative of an open-shell singlet state in which an electron (or ligand) is detached and the need for multi-reference treatment. However, because the geometry, total energy, and expectation value of the S^2 operator were reproduced by an unrestricted broken symmetry calculation, the positive eigenvalues could also be an effect of basis set deficiency rather than limitations inherent to the single-determinant DFT M06-2X method. Nevertheless, our results for $[Bi(N_3)_6]^{3-}$ are approximate.

The $[Bi(N_3)_6]^{3-}$ ion is extremely fluxional with many closely spaced PES minima. The predicted minimum-energy gas-phase structure deviates from the experimental solid-state X-ray crystal structure

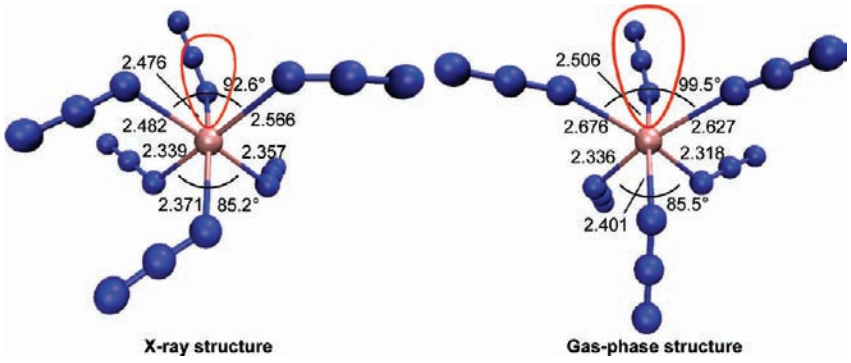

Figure 18. Comparison of the solid-state $[P(C_6H_5)^+]_3$ salt structure and computed gas-phase structure of the fluxional $[Bi(N_3)_6]^{3-}$ ion showing significant solid-state effects. The difference in the effective size of the lone valence electron pair (red) is explained by its increased activity in the gas phase. The depicted angles are the cone angles, i.e., the average of the three dihedral angles in each cone.

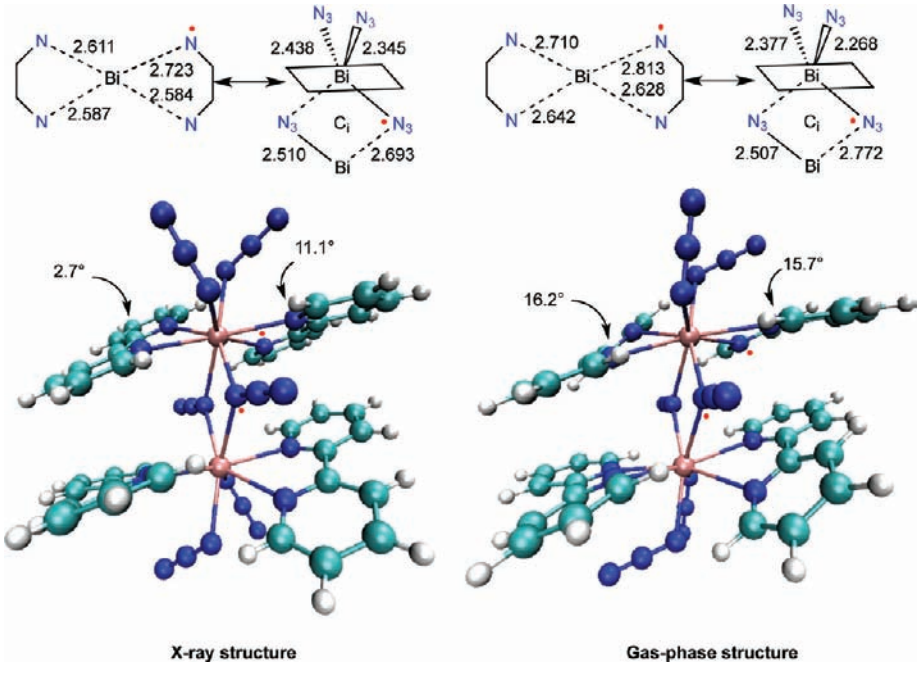

Figure 19. Solid-state and gas-phase structures of $[(bipy)_2{\cdot}Bi(N_3)_3]_2$.

dx.doi.org/10.1021/ic202307a | Inorg. Chem. 2012, 51, 1127–1141

(Figure 18). In both cases, the lone valence electron pair on bismuth is sterically active, resulting in monocapped octahedral structures. The cone angle of the capped trigonal pyramid increases from 92.6° in the solid state to 99.5° in the free ion. As a consequence of the increased cone angle, the Bi−N bonds of this cone are also longer. Thus, the cations in the crystal lattice appear to partially deactivate the lone valence electron pair of bismuth.

$[(bipy)_2{\cdot}Bi(N_3)_3]_2$. The large size (500 explicit electrons) of the C_i-symmetric neutral $[(bipy)_2{\cdot}Bi(N_3)_3]_2$ complex permitted only optimization at the double-ζ level (see the Computational Details section). At this computational level, the only major structural changes relative to the X-ray crystal structure were small increases of the 2,2′-bipyridine twist angles, from 2.7° and 11.1° to 15.7° and 16.2°, respectively (Figure 19). Because of the high CN enforced by the square-antiprismatic structure of $[(bipy)_2{\cdot}Bi(N_3)_3]_2$, the lone valence electron pairs are sterically inactive, both in the solid state and in the gas phase.

CONCLUSIONS

A systematic study of bismuth polyazides has been carried out in our laboratory. In addition to more details on $Bi(N_3)_3$, $[Bi(N_3)_4]^-$, and $[Bi(N_3)_6]^{3-}$, which have recently also been independently studied by others,[23,24] the novel dianion $[Bi(N_3)_5]^{2-}$ and the 2,2′-bipyridine adducts, $[(bipy)_2{\cdot}Bi(N_3)_3]_2$ and $[bipy{\cdot}Bi(N_3)_5]^{2-}$, were prepared and structurally characterized. For comparison, the analogous $bipy{\cdot}As(N_3)_3$ and $bipy{\cdot}Sb(N_3)_3$ adducts were also prepared and structurally characterized. It is shown that the solid-state structures of the bismuth azides generally differ from those found for the corresponding lighter pnictogen compounds because of bismuth's tendency to form higher CNs. The pnictogens can increase their CNs either by association, i.e., sharing nitrogen atoms through the formation of intermolecular nitrogen bridges, by anion formation, i.e., the addition of azide ions, or by adduct formation with Lewis bases. Anion or adduct formation also reduces the high shock sensitivity of the neutral parent molecules and renders them more manageable. The basic building blocks for intermolecular association are four-membered Bi_2N_2 parallelograms. Isolated parallelograms result in the formation of dimers, while two bridging parallelograms attached to the same pnictogen atom produce a polymeric band structure, and three bridging parallelograms result in a polymeric sheet structure. The shape of the three bridging parallelograms closely resembles that of the Mitsubishi emblem and, therefore, this structural element has been termed a "Mitsubishi".[9] Because the III+ oxidation state pnictogens possess one lone valence electron pair, this pair can contribute to the CN by becoming sterically active. The lone pair is sterically active in the $[M(N_3)_4]^-$ (M = As, Sb, Bi), $[Bi(N_3)_5]^{2-}$, and $[Bi(N_3)_6]^{3-}$ anions and the $As(N_3)_3$ and $Sb(N_3)_3$ molecules but inactive in $(bipy)_2{\cdot}Bi(N_3)_3$ and solid $[bipy{\cdot}Bi(N_3)_5]^{2-}$. The $(bipy)_2{\cdot}Bi(N_3)_3$ molecule possesses a rather unique structure of a dimer consisting of two square antiprisms with CN 8 that are coupled through a Bi_2N_2 parallelogram.

Because all of these polyazido compounds are highly fluxional, many conformers with very similar energies can exist. Therefore, very small changes in packing and lattice energies can not only dramatically impact their solid-state structures but also influence the steric activity of lone valence electron pairs. For this reason, great care must be exercised when comparing such structures.

Modern DFT calculations were used to predict the structures of the free gaseous species devoid of solid-state or solution effects. The hybrid meta exchange-correlation DFT M06-2X method appears well suited for the reliable prediction of the steric activity of the lone valence electron pair in these types of main-group compounds.

The solid-state structures can significantly differ from those of the free gas-phase species or the ones in solution. Our results suggest that lone valence electron pairs that are sterically inactive in the solid state can become sterically active in the gas phase. This lone pair activation, "LPA", is in sharp contrast to the usually observed symmetry enhancement in either solution or the gas-phase in which distortions induced by solid-state or lattice effects are removed.

The reduction of the steric activity of the lone valence electron pair in an LPA species due to changes in its chemical environment can be attributed to positively charged counterions or polar solvents allowing for more electron density on the ligands, thereby reducing the repulsion experienced by the lone pair in the center of the molecule and increasing the repulsion between the more negatively charged ligands. For "LPA" to occur, the involved species should possess a lone valence electron pair, be at the limit of its maximum CN, and, because of the relative weakness of the effect of the chemical environment, have two or more conformers that are close in energy.

Experimental proof for the LPA effect might not be trivial because determination of the gas-phase structures of multiply charged LPA-type anions is experimentally challenging. Because the structures in solvents are expected to more closely resemble those of the free gas-phase species, it might be more feasible to search for compounds that exhibit a sterically inactive lone valence electron pair in the solid state and a sterically active lone pair in solution. Our results suggest that $[bipy{\cdot}Bi(N_3)_5]^{2-}$ might be a good candidate for such a study.

ASSOCIATED CONTENT

Supporting Information

Figures S1−S19 and Tables S1−S37. This material is available free of charge via the Internet at http://pubs.acs.org.

AUTHOR INFORMATION

Corresponding Author

*E-mail: haiges@usc.edu (R.H.), rahm@usc.edu (M.R.), kchriste@usc.edu (K.O.C.).

ACKNOWLEDGMENTS

This work was supported by the National Science Foundation, the Office of Naval Research, the Air Force Office of Scientific Research, the Defense Threat Reduction Agency, and the Department of Energy. D.A.D. is indebted to the Robert Ramsay Endowment of the University of Alabama. Computational work at the University of Southern California was supported by the University of Southern California Center for High-Performance Computing and Communications.

DEDICATION

†Dedicated to Professor George Olah on the occasion of his 84th birthday.

REFERENCES

(1) (a) Kornath, A. *Angew. Chem., Int. Ed.* **2001**, *40*, 3135. (b) Fraenk, W.; Klapötke, T. M. In *Inorganic Chemistry Highlights*; Meyer, G., Naumann, D., Wesemann, L., Eds.; Wiley-VCH: Weinheim, Germany, 2002. (c) Müller, J. *Coord. Chem. Rev.* **2002**, *235*, 105. (d) Knapp, C.; Passmore, J. *Angew. Chem., Int. Ed.* **2004**, *43*, 4834.

(2) Neumüller, B.; Schmock, F.; Dehnicke, K. *Z. Anorg. Allg. Chem.* **1999**, *625*, 1243.
(3) Filippou, A. C.; Portius, P.; Neumann, D. U.; Wehrstedt, K.-D. *Angew. Chem., Int. Ed.* **2000**, *39*, 4333.
(4) Filippou, A. C.; Portius, P.; Schnakenburg, G. *J. Am. Chem. Soc.* **2002**, *124*, 12396.
(5) Klapötke, T. M.; Krumm, B.; Mayer, P.; Pietrowski, H.; Ruscitti, O. P.; Schiller, A. *Inorg. Chem.* **2002**, *41*, 1184.
(6) Karaghiosoff, K.; Klapötke, T. M.; Krumm, B.; Nöth, H.; Schütt, T.; Suter, M. *Inorg. Chem.* **2002**, *41*, 170.
(7) Klapötke, T. M.; Krumm, B.; Mayer, P.; Schwab, I. *Angew. Chem., Int. Ed.* **2003**, *42*, 5843.
(8) Haiges, R.; Boatz, J. A.; Vij, A.; Gerken, M.; Schneider, S.; Schroer, T.; Christe, K. O. *Angew. Chem., Int. Ed.* **2003**, *42*, 5847.
(9) Haiges, R.; Vij, A.; Boatz, J. A.; Schneider, S.; Schroer, T.; Gerken, M.; Christe, K. O. *Chem.—Eur. J.* **2004**, *10*, 508.
(10) Haiges, R.; Schneider, S.; Schroer, T.; Christe, K. O. *Angew. Chem., Int. Ed.* **2004**, *43*, 4919.
(11) Haiges, R.; Boatz, J. A.; Vij, A.; Vij, V.; Gerken, M.; Schneider, S.; Schroer, T.; Yousufuddin, M.; Christe, K. O. *Angew. Chem., Int. Ed.* **2004**, *43*, 6676.
(12) (a) Buder, W.; Schmidt, A. *Z. Anorg. Allg. Chem.* **1975**, *415*, 263. (b) Volgnandt, P.; Schmidt, A. *Z. Anorg. Allg. Chem.* **1976**, *425*, 189. (c) Portius, P.; Fowler, P. W.; Adams, H.; Todorova, T. Z. *Inorg. Chem.* **2008**, *47*, 12004. (d) Klapötke, T. M.; Geissler, P. *J. Chem. Soc., Dalton Trans.* **1995**, 3365. (e) Geissler, P.; Klapötke, T. M. *Spectrochim. Acta, Part A* **1995**, *51*, 1075. (f) Klapötke, T. M.; Nöth, H.; Schuett, T.; Warchhold, M. *Angew. Chem., Int. Ed.* **2000**, *39*, 2108. (g) Klapötke, T. M.; Schulz, A.; McNamara, A. *J. Chem. Soc., Dalton Trans.* **1996**, 2985.
(13) Haiges, R.; Boatz, J. A.; Schneider, S.; Schroer, T.; Yousufuddin, M.; Christe, K. O. *Angew. Chem., Int. Ed.* **2004**, *43*, 3148.
(14) Haiges, R.; Boatz, J. A.; Bau, R.; Schneider, S.; Schroer, S.; Yousufuddin, M.; Christe, K. O. *Angew. Chem., Int. Ed.* **2005**, *44*, 1860.
(15) Haiges, R.; Boatz, J. A.; Schroer, T.; Yousufuddin, M.; Christe, K. O. *Angew. Chem., Int. Ed.* **2006**, *45*, 4830.
(16) Haiges, R.; Boatz, J. A.; Yousufuddin, M.; Christe, K. O. *Angew. Chem., Int. Ed.* **2007**, *46*, 2869.
(17) Johnson, J. P.; MacLean, G. K.; Passmore, J.; White, P. S. *Can. J. Chem.* **1989**, *67*, 1687.
(18) Crawford, M. J.; Ellern, A.; Mayer, P. *Angew. Chem., Int. Ed.* **2005**, *44*, 7874.
(19) Klapötke, T. M.; Krumm, B.; Scherr, M.; Haiges, R.; Christe, K. O. *Angew. Chem., Int. Ed.* **2007**, *46*, 8686.
(20) Haiges, R.; Boatz, J. A.; Christe, K. O. *Angew. Chem., Int. Ed.* **2010**, *49*, 8008.
(21) Klapötke, T. M.; Schulz, A. *Main Group Met. Chem.* **1997**, *20*, 325.
(22) Portius, P.; Filippou, A. C.; Schnakenburg, G.; Davis, M.; Wehrstedt, K. D. *Angew. Chem., Int. Ed.* **2010**, *49*, 8013.
(23) Villinger, A.; Schulz, A. *Angew. Chem., Int. Ed.* **2010**, *49*, 8017.
(24) Schulz, S.; Lyhs, B.; Jansen, G.; Bläser, D.; Wölper, C. *Chem. Commun.* **2011**, *47*, 3401.
(25) Haiges, R.; Schroer, T.; Yousufuddin, M.; Christe, K. O. *Z. Anorg. Allg. Chem.* **2005**, *631*, 2691.
(26) (a) *SMART V 5.625, Software for the CCD Detector System*; Bruker AXS: Madison, WI, 2001. (b) *SAINT V 6.22, Software for the CCD Detector System*; Bruker AXS: Madison, WI, 2001. (c) *SADABS, Software for the CCD Detector System*; Bruker AXS: Madison, WI, 2001. (d) Sheldrick, G. M. *SHELXS-90, Program for the Solution of Crystal Structure*; University of Göttingen: Göttingen, Germany, 1990. (f) *SHELXL-97, Program for the Refinement of Crystal Structure*; University of Göttingen: Göttingen, Germany, 1997. (e) *SHELXTL 6.12 for Windows NT/2000, Program library for Structure Solution and Molecular Graphics*; Bruker AXS: Madison, WI, 2000.
(27) (a) *Bruker Instrument Service v2011.4.0.0*; Bruker AXS: Madison, WI, 2011. (b) *SAINT V7.68A*; Bruker AXS: Madison, WI, 2009. (c) *SADABS V2008/1*; Bruker AXS: Madison, WI, 2008. (d) *Bruker SHELXTL V2011.4-0*; Bruker AXS: Madison, WI, 2011. (e) Sheldrick, G. M. *Acta Crystallogr.* **2008**, *A64*, 112−122.
(28) Farrugia, L. J. *J. Appl. Crystallogr.* **1997**, *30*, 565.
(29) Zhao, Y.; Truhlar, D. G. *Theor. Chem. Acc.* **2008**, *120*, 215.
(30) Frisch, M. J.; Trucks, G. W.; Schlegel, H. B.; Scuseria, G. E.; Robb, M. A.; Cheeseman, J. R.; Scalmani, G.; Barone, V.; Mennucci, B.; Petersson, G. A.; Nakatsuji, H.; Caricato, M.; Li, X.; Hratchian, H. P.; Izmaylov, A. F.; Bloino, J.; Zheng, G.; Sonnenberg, J. L.; Hada, M.; Ehara, M.; Toyota, K.; Fukuda, R.; Hasegawa, J.; Ishida, M.; Nakajima, T.; Honda, Y.; Kitao, O.; Nakai, H.; Vreven, T.; Montgomery, J. J. A.; Peralta, J. E.; Ogliaro, F.; Bearpark, M.; Heyd, J. J.; Brothers, E.; Kudin, K. N.; Staroverov, V. N. K. R.; Normand, J.; Raghavachari, K.; Rendell, A.; Burant, J. C.; Iyengar, S. S.; Tomasi, J.; Cossi, M.; Rega, N.; Millam, N. J.; Klene, M.; Knox, J. E.; Cross, J. B.; Bakken, V.; Adamo, C.; Jaramillo, J.; Gomperts, R.; Stratmann, R. E.; Yazyev, O.; Austin, A. J.; Cammi, R.; Pomelli, C.; Ochterski, J. W.; Martin, R. L.; Morokuma, K.; Zakrzewski, V. G.; Voth, G. A.; Salvador, P.; Dannenberg, J. J.; Dapprich, S.; Daniels, A. D.; Farkas, Ö.; Foresman, J. B.; Ortiz, J. V.; Cioslowski, J.; Fox, D. J. *Gaussian 09*, revision A.1; Gaussian, Inc.: Wallingford, CT, 2009.
(31) Zhao, Y.; Truhlar, D. G. *J. Chem. Theory Comput.* **2011**, *7*, 669.
(32) Valero, R.; Gomes, J. R. B.; Truhlar, D. G.; Illas, F. *J. Chem. Phys.* **2008**, *129*, 124710/1.
(33) Dixon, D. A.; Grant, D. J.; Christe, K. O.; Peterson, K. A. *Inorg. Chem.* **2008**, *47*, 5485.
(34) Tomasi, J.; Mennucci, B.; Cammi, R. *Chem. Rev.* **2005**, *105*, 2999.
(35) Peterson, K. A.; Yousaf, K. E. *J. Chem. Phys.* **2010**, *133*, 174116/1.
(36) Dunning, T. H. Jr. *J. Chem. Phys.* **1989**, *90*, 1007.
(37) Crystal data for $C_{24}H_{20}BiN_{12}P$: M_r = 716.47, monoclinic, space group $P2(1)/c$, a = 8.1937(6) Å, b = 24.0269(18) Å, c = 13.5750(10) Å, α = 90°, β = 90.9850(10)°, γ = 90°, V = 2672.1(3) Å^3, $F(000)$ = 1384, ρ_{calcd} (Z = 4) = 1.781 g·cm^{-3}, μ = 6.696 mm^{-1}, approximate crystal dimensions 0.25 × 0.16 × 0.14 mm^3, θ range = 1.70−27.52°, Mo Kα (λ = 0.710 73 Å), T = 133(2) K, 23 086 measured data of which 6086 (R_{int} = 0.0287) are unique. Lorentz and polarization correction, absorption correction, structure solution by the Patterson method, and full-matrix least-squares refinement on F^2. Data to parameters ratio: 17.7:1. Final R indices [$I > 2\sigma(I)$]: R1 = 0.0236, wR2 = 0.0469. R indices (all data): R1 = 0.0327, wR2 = 0.0502. GOF on F^2 = 1.037. Further crystallographic details can be obtained from the Cambridge Crystallographic Data Centre, 12 Union Road, Cambridge CB21EZ, U.K. [fax (+44) 1223-336-033; e-mail deposit@ccdc.cam.ac.uk] upon quoting the deposition number CCDC 771004.
(38) Crystal data for $C_{72}H_{60}BiN_{17}P_4$: M_r = 1496.23, orthorhombic, space group $Pca2(1)$, a = 19.9400(17) Å, b = 20.0602(17) Å, c = 16.6929(15) Å, α = 90°, β = 90°, γ = 90°, V = 6677.2(10) Å^3, $F(000)$ = 3016, ρ_{calcd} (Z = 4) = 1.488 g·cm^{-3}, μ = 2.794 mm^{-1}, approximate crystal dimensions 0.21 × 0.20 × 0.18 mm^3, θ range = 1.44−27.50°, Mo Kα (λ = 0.710 73 Å), T = 173(2) K, 40 412 measured data of which 12 988 (R_{int} = 0.0885) are unique. Lorentz and polarization correction, absorption correction, structure solution by the Patterson method, and full-matrix least-squares refinement on F^2. Data to parameters ratio: 15.3:1. Final R indices [$I > 2\sigma(I)$]: R1 = 0.0507, wR2 = 0.1088. R indices (all data): R1 = 0.0732, wR2 = 0.1145. GOF on F^2 = 1.015. Further crystallographic details can be obtained from the Cambridge Crystallographic Data Centre, 12 Union Road, Cambridge CB21EZ, U.K. [fax (+44) 1223-336-033; e-mail deposit@ccdc.cam.ac.uk] upon quoting the deposition number CCDC 771005.
(39) Greenwood, N. N.; Earnshaw, A. *Chemistry of the Elements*; Butterworth-Heinemann: Oxford, 1998.
(40) Christe, K. O.; Curtis, E. C.; Schack, C. J.; Pilipovich, D. *Inorg. Chem.* **1972**, *11*, 1679.
(41) (a) Pimentel, G. C. *J. Chem. Phys.* **1951**, *19*, 446. (b) Hach, R. J.; Rundle, R. E. *J. Am. Chem. Soc.* **1951**, *73*, 4321. (c) Rundle, R. E. *J. Am. Chem. Soc.* **1963**, *85*, 112.
(42) Crystal data for $C_{58}H_{48}BiN_{17}P_2$: M_r = 1254.05, monoclinic, space group $P2(1)/n$, a = 11.798(2) Å, b = 22.286(4) Å, c = 21.024(4) Å, α =

90°, β = 102.078(3)°, γ = 90°, V = 5405.3(16) Å^3, F(000) = 2512, ρ_{calcd} (Z = 4) = 1.541 g·cm^{-3}, μ = 3.378 mm^{-1}, approximate crystal dimensions 0.33 × 0.30 × 0.15 mm^3, θ range = 1.35−27.51°, Mo Kα(λ = 0.710 73 Å), T = 113(2) K, 32 987 measured data of which 12 033 (R_{int} = 0.0442) are unique. Lorentz and polarization correction, absorption correction, structure solution by the Patterson method, and full-matrix least-squares refinement on F^2. Data to parameters ratio: 16.5:1. Final R indices [$I > 2\sigma(I)$]: R1 = 0.0369, wR2 = 0.0871. R indices (all data): R1 = 0.0507, wR2 = 0.0986. GOF on F^2 = 1.012. Further crystallographic details can be obtained from the Cambridge Crystallographic Data Centre, 12 Union Road, Cambridge CB21EZ, U.K. [fax (+44) 1223-336-033; e-mail deposit@ccdc.cam.ac.uk] upon quoting the deposition number CCDC 843233.

(43) Favas, M. C.; Harrowfield, J. M.; Kepert, D. L.; Skelton, B. W.; Vitolo, L. M.; White, A. H. *Aust. J. Chem.* **1992**, *45*, 1547.

(44) Gillespie, R. J.; Hargittai, I. *The VSEPR Model of Molecular Geometry*; Allin and Bacon: Needham Heights, MA, 1991.

(45) Crystal data for $C_{72}H_{60}BiN_{18}P_3$: M_r = 1479.27, monoclinic, space group $P2(1)/n$, a = 13.3429(9) Å, b = 22.6779(16) Å, c = 22.0466(15) Å, α = 90°, β = 96.9480(10)°, γ = 90°, V = 6622.1(8) Å^3, F(000) = 2984, ρ_{calcd} (Z = 4) = 1.484 g·cm^{-3}, μ = 2.794 mm^{-1}, approximate crystal dimensions 0.30 × 0.17 × 0.14 mm^3, θ range = 1.29−27.46°, Mo Kα (λ = 0.710 73 Å), T = 143(2) K, 56 213 measured data of which 14 939 (R_{int} = 0.0656) are unique. Lorentz and polarization correction, absorption correction, structure solution by the Patterson method, and full-matrix least-squares refinement on F^2. Data to parameters ratio: 17.3:1. Final R indices [$I > 2\sigma(I)$]: R1 = 0.0413, wR2 = 0.0712. R indices (all data): R1 = 0.0764, wR2 = 0.0802. GOF on F^2 = 1.038. Further crystallographic details can be obtained from the Cambridge Crystallographic Data Centre, 12 Union Road, Cambridge CB21EZ, U.K. [fax (+44) 1223-336-033; e-mail deposit@ccdc.cam.ac.uk] upon quoting the deposition number CCDC 771006.

(46) Haiges, R.; Vij, A.; Christe, K. O. Unpublished observations.

(47) Crystal data for $C_{10}H_8AsN_{11}$: M_r = 357.19, monoclinic, space group $P2(1)/c$, a = 7.1835(7) Å, b = 18.7740(17) Å, c = 10.6709(10) Å, α = 90°, β = 108.6600(10)°, γ = 90°, V = 1363.5(2) Å^3, F(000) = 712, ρ_{calcd} (Z = 4) = 1.740 g·cm^{-3}, μ = 2.510 mm^{-1}, approximate crystal dimensions 0.51 × 0.47 × 0.41 mm^3, θ range = 2.17−28.42°, Mo Kα (λ = 0.710 73 Å), T = 100(2) K, 18 248 measured data of which 3416 (R_{int} = 0.0339) are unique. Lorentz and polarization correction, absorption correction, structure solution by direct methods, and full-matrix least-squares refinement on F^2. Data to parameters ratio: 17.2:1. Final R indices [$I > 2\sigma(I)$]: R1 = 0.0222, wR2 = 0.0510. R indices (all data): R1 = 0.0262, wR2 = 0.0522. GOF on F^2 = 1.082. Further crystallographic details can be obtained from the Cambridge Crystallographic Data Centre, 12 Union Road, Cambridge CB21EZ, U.K. [fax (+44) 1223-336-033; e-mail deposit@ccdc.cam.ac.uk] upon quoting the deposition number CCDC 843234.

(48) Crystal data for $C_{10}H_8N_{11}Sb$: M_r = 404.02, monoclinic, space group $P2(1)/c$, a = 7.23230(10) Å, b = 18.6697(2) Å, c = 10.50710(10) Å, α = 90°, β = 107.2700(10)°, γ = 90°, V = 1354.76(3) Å^3, F(000) = 784, ρ_{calcd} (Z = 4) = 1.981 g·cm^{-3}, μ = 2.054 mm^{-1}, approximate crystal dimensions 0.34 × 0.22 × 0.10 mm^3, θ range = 2.18−33.29°, Mo Kα (λ = 0.710 73 Å), T = 100(2) K, 90 100 measured data of which 5228 (R_{int} = 0.0382) are unique. Lorentz and polarization correction, absorption correction, structure solution by direct methods, and full-matrix least-squares refinement on F^2. Data to parameters ratio: 26.3:1. Final R indices [$I > 2\sigma(I)$]: R1 = 0.0148, wR2 = 0.0343. R indices (all data): R1 = 0.0185, wR2 = 0.0356. GOF on F^2 = 1.068. Further crystallographic details can be obtained from the Cambridge Crystallographic Data Centre, 12 Union Road, Cambridge CB21EZ, U.K. [fax (+44) 1223-336-033; e-mail deposit@ccdc.cam.ac.uk] upon quoting the deposition number CCDC 843231.

(49) Bondi, A. *J. Phys. Chem.* **1964**, *68*, 441.

(50) Crystal data for $C_{40}H_{32}Bi_2N_{26}$: M_r = 1294.88, monoclinic, space group $P2(1)/n$, a = 8.9891(5) Å, b = 22.1991(12) Å, c = 10.9374(6) Å, α = 90°, β = 103.6040(10)°, γ = 90°, V = 2121.3(2) Å^3, F(000) = 1240, ρ_{calcd} (Z = 2) = 2.027 g·cm^{-3}, μ = 8.352 mm^{-1}, approximate crystal dimensions 0.22 × 0.13 × 0.09 mm^3, θ range = 2.12−27.49°, Mo Kα (λ = 0.710 73 Å), T = 103(2) K, 12 973 measured data of which 4785 (R_{int} = 0.0348) are unique. Lorentz and polarization correction, absorption correction, structure solution by the Patterson method, and full-matrix least-squares refinement on F^2. Data to parameters ratio: 15.6:1. Final R indices [$I > 2\sigma(I)$]: R1 = 0.0282, wR2 = 0.0599. R indices (all data): R1 = 0.0356, wR2 = 0.0630. GOF on F^2 = 1.065. Further crystallographic details can be obtained from the Cambridge Crystallographic Data Centre, 12 Union Road, Cambridge CB21EZ, U.K. [fax (+44) 1223-336-033; e-mail deposit@ccdc.cam.ac.uk] upon quoting the deposition number CCDC 843232.

(51) Christe, K. O.; Sanders, J. C. P.; Schrobilgen, G. J.; Wilson, W. W. *Chem. Commun.* **1991**, 837.

(52) Mahjoub, A. R.; Seppelt, K. *Angew. Chem., Int. Ed.* **1991**, *30*, 876.

(53) Grant, D. J.; Wang, T.-H.; Dixon, D. A.; Christe, K. O. *Inorg. Chem.* **2010**, *49*, 261.

(54) Drake, G. W.; Dixon, D. A.; Sheehy, J. A.; Boatz, J. A.; Christe, K. O. *J. Am. Chem. Soc.* **1998**, *120*, 8392.

(55) Fischer, R. A.; Miehr, A.; Herdtweck, E.; Mattner, M. R.; Ambacher, O.; Metzger, T.; Born, E.; Weinkauf, S.; Pulham, C. R.; Parsons, S. *Chem.—Eur. J.* **1996**, *2*, 1353.